Solute drag modeling for ferrite growth kinetics during precipitation experiments

I.-E. Benrabah, H.P Van Landeghem, F. Bonnet, B. Denand, G. Geandier, A. Deschamps

Solute drag modeling for ferrite growth kinetics during precipitation experiments

I.-E. Benrabah[a,*], H.P Van Landeghem[a], F. Bonnet[b], B. Denand[c], G. Geandier[c], A. Deschamps[a]

[a] *Univ. Grenoble Alpes, CNRS, Grenoble INP, SIMAP, F-38000 Grenoble, France.*
[b] *ArcelorMittal Research, F-57280 Maizières-lès-Metz, France.*
[c] *Université de Lorraine, CNRS, IJL, F-54000 Nancy, France.*

Abstract

The growth kinetics of ferrite during intercritical annealing of steel has been investigated using *in situ* high energy X-ray diffraction with a specially designed furnace allowing highly quantitative measurements of phase volume fractions. Kinetics have been obtained at 730°C, 750°C and 775°C in different ternary Fe-C-X (where X : Mn, Ni, Mo and Cr) alloys and in a quaternary Fe-C-1Mn-1Cr (wt.%) alloy. The obtained results were compared with the predictions of classical Local Equilibrium and Para-Equilibrium models as well as an improved version of a three-jump solute drag model, where the interactions between the solute elements and the moving interface are described comprehensively. Good agreement was obtained between the measured ferrite growth kinetics and the predictions of the solute drag model for the different Fe-C-X systems using only one fitting parameter, namely the Fe-X interaction parameter at the interface. The interactions found here qualitatively match those reported in literature for all solutes except for Ni, which displayed an attractive interaction with the interface. For the quaternary Fe-C-Mn-Cr system, the solute drag model succeeded in predicting ferrite growth kinetics using the same interaction values as used for the ternary Fe-C-Mn and Fe-C-Cr systems.

Keywords: Steels, Ferrite growth, Solute drag, Interface

1. Introduction

Tailoring microstructures by means of solid-solid phase transformations and adapting chemical compositions is the main avenue to control mechanical properties in steels. Among a large variety of solid state phase transformations, austenite-to-ferrite has been the most studied reaction from both technological and scientific standpoints [1, 2, 3, 4, 5, 6]. Ferrite growth kinetics in steels is highly conditioned by the partitioning behavior of substitutional alloying elements between the parent and child phases. This is due to the low diffusivity of these elements compared to interstitial elements, notably carbon. As a result, the transformation can proceed with either full or negligible partitioning

*corresponding author
Email address: imededdine.benrabah@gmail.com (I.-E. Benrabah)

of the substitutional elements between the growing ferrite and austenite [7, 2]. In the former case, the transformation kinetics is controlled by their slow diffusion (LEP mode), whereas in the latter, it is mainly dictated by the much faster diffusion of carbon. Two models representing the limit cases of negligible partitioning transformations known as para-equilibrium (PE) and local equilibrium with negligible partitioning (LENP) have been proposed to describe the rate of austenite to ferrite transformation in ternary and higher order systems [8, 9, 10, 2]. Both models were used to successfully predict ferrite growth in ternary Fe-C-X systems under particular conditions of temperature and composition [11, 6, 5, 3]. However, experimental observations showed a more complex behavior of the interface conditions during ferrite growth in some systems where such models failed to predict the measured growth kinetics. One of the theories generally invoked to explain the mentioned discrepancies between calculated and measured kinetics is that substitutional element interactions with the moving (α/γ) interface lead to a dissipation of the available driving force and thus, to a retardation of ferrite growth. The so-called 'Solute Drag effect' (SD) involves solute segregation at the mobile (α/γ) interface, thereby reducing its velocity. The solute drag based models display a better aptitude at predicting kinetics for broad ranges of composition and temperature in ternary systems. The three-jump solute drag based model was proposed by Zurob et al. [12] to describe ferrite growth kinetics in Fe-C-X alloys using the dissipation approach developed by Hillert and Sundman [13]. Zurob's model was applied to a large kinetic dataset from decarburization experiments in ternary Fe-C-X systems (X : Mn, Ni, Mo, Co, Si, Cr ...) [12, 14]. In most cases, good agreement was obtained between the experimental results and the predicted ferrite growth kinetics. In multicomponent systems, the segregation behavior of solute elements at the interface becomes more complex [15, 16]. The simultaneous presence of multiple solutes at the interface may affect the interaction behavior of each element with the moving interface [17]. Beside the solute-interface interaction of each solute element, inter-elemental interactions must be considered when modeling growth kinetics in Fe-C-X_1-X_2 systems, giving rise to the so-called 'coupled-solute drag effect' [15, 18, 19]. Carbon is reported to segregate at the interface [20] and thus, it is important to consider its interactions with substitutional elements. These can vary drastically, from strongly repulsive to strongly attractive, and result in complex segregation behaviors when three elements (X_1,X_2,C) or more are present.The XC interaction effect on the dissipated energy due to solute drag was evaluated by Enomoto et al.[21] and Guo et al.[22] for different Fe-X-C systems. Results showed that this parameter plays an important role in the segregation behavior of the substitutional elements at the austenite/ferrite interface. In Zurob's approach [12], the only modified parameter to express the mutual interaction between elements at the interface is the Fe-X interaction parameter (using L parameters from ThermoCalc database). However, modifying this parameter can implicitly lead to an effective change in the Wagner interaction parameter between X_1 and X_2[23]. Moreover, experimental observations show that carbon segregates at the transformation interface [24, 25], a phenomenon that was not accounted for in Zurob's original version of the three-jump model. Thus, a more in-depth study is needed on the effect of interaction terms on the apparent binding energy and thus the segregation behavior of solute elements at the interface. In the declinations of the three-jump solute drag model reported so far, the effect of these interactions on the segregation behavior of solute elements at the interface has not been integrated. Based on these experimental observations as well as Enomoto

et al.[21] and Guo et al.[22] works, we propose in the present study, the integration of the different interaction parameters to the three-jumps solute drag model.

The three-jump model has, until now, been mostly applied to the simulation of ferrite growth during decarburization experiments [12, 16, 15, 14, 26], where the progression rate of the transformation front is obtained by metallography. There are only few reports comparing experimental precipitation kinetics and solute drag modelling, although precipitation is more representative of the microstructural evolution in industrial conditions. This is mainly due to the difficulty to obtain high quality measurements of ferrite growth kinetics using standard metallography due to stereological and sectioning effects [27, 28]. Dilatometry offers the advantage of an *in situ* investigation of phase transformations in steels [29, 30, 31, 32]. However, obtaining quantitative data from this method relies on assumptions regarding, notably, the austenite and ferrite lattice parameters and their evolutions during phase transformation [30]. Alternatively, high energy X-Ray diffraction (HEXRD), performed using a synchrotron X-ray source, can be used to obtain accurate quantitative data on the transformation, especially the nature of phases and their respective fractions [33, 34, 32, 35], provided that a sufficient number of grains is illuminated by the X-ray beam to ensure powder diffraction conditions. By coupling this method with the appropriate sample environment, phase transformation kinetics can be studied with sub-second time resolution.

In the present work, ferrite precipitation kinetics have been investigated using HEXRD in ternary Fe-C-X and quaternary Fe-C-X_1-X_2 systems. Different substitutional elements were considered (Mn, Ni, Mo and Cr), in order to determine their interaction with the moving interface. Varying temperature and solute content enabled the evaluation of their effects on the transformation kinetics. The experimental results were compared to the predictions of a modified version of the solute drag model developed by Zurob et al.[12], which accounts for the interaction of carbon with the interface, as well as for the interaction of the various solutes at the interface.

2. Material and methods

The materials used in this study were cast, hot-rolled and homogenized at 1200°C for 18 h and their precise initial composition is provided in Table 1. Cylindrical samples with a 30 mm length and a 3 mm diameter were cut from the billets. The samples were austenized at 910°C for 1 min and quenched into water to obtain a martensitic microstructure.

Table 1: Chemical composition (wt. %) of the different alloys used to investigate ferrite growth kinetics using HEXRD experiments. The measurements were realized by Spark-OES method.

Composition %wt	C	Si	Mn	Mo	Cr	Ni	Al	Other	Fe
Fe-C-1Mn	0.26	0.029	0.98	<0.002	<0.002	<0.002	0.003	<0.002	Bal.
Fe-C-0.7Mn	0.26	0.03	0.7	<0.002	<0.002	<0.002	0.003	<0.002	Bal.
Fe-C-0.3Mn	0.26	0.03	0.3	<0.002	<0.002	<0.002	0.003	<0.002	Bal.
Fe-C-0.2Mo	0.26	0.019	0.004	0.21	<0.002	<0.002	0.003	<0.002	Bal.
Fe-C-1Ni	0.22	0.02	0.004	<0.002	<0.002	1.05	0.003	<0.002	Bal.
Fe-C-1Cr	0.26	0.027	0.004	<0.002	0.98	<0.002	0.003	<0.002	Bal.
Fe-C-1Mn-1Cr	0.26	0.02	0.98	<0.002	1.01	<0.002	0.006	<0.002	Bal.

In situ High energy X-ray diffraction experiments were performed at the beamline P21.2 of the DESY PETRA III synchrotron in Hamburg, Germany, using an energy of 82 keV (λ = 0.1512 Å). The high-energy beam allows to obtain diffraction data in transmission. To maximize the number of grains in the illuminated volume, a beam size of 0.5 x 0.5 mm^2 was used. The Debye-Scherrer diffraction rings were collected using a high-resolution 2D VAREX 4343CT detector with a 10 Hz acquisition rate placed 1 m away from the sample. The cylindrical samples were heated using a radiative heating furnace specially developed to perform thermal treatments with a controlled rotation of the sample (Fig.1)[36]. This controlled rotation drastically increases the number of grains in diffraction conditions during the measurements, thereby approaching random powder diffraction conditions and ensuring the quantitative character of the phase fraction measurements. The rotation speed was set at 5 full rotations per second, leading to a 180° rotation per detector frame. Heating was achieved by a set of lamps surrounding the sample and the temperature was regulated using a type-S thermocouple spot-welded on the sample, close to the beam path. An argon flow of 0.4 $l.min^{-1}$ was used to limit decarburization and oxidation during the experiments.

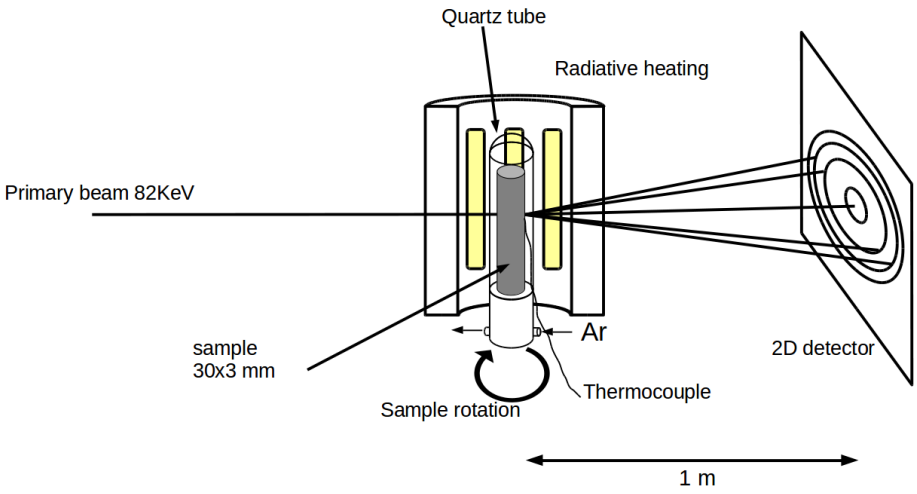

Figure 1: Diagram of the experimental setup used for HEXRD experiments. A rotation system was used to maximize the number of analyzed grains in the diffracted volume.

The details of the heat treatments for *in situ* HEXRD experiments were as follows. The samples were heated to 910°C at 10°C/s and held for 30 s at this temperature to reach complete austenitization, which was checked using the diffraction patterns recorded during this step. Samples were then rapidly cooled at 60°C/s down to the inter-critical temperature (730°C, 750°C, and 775°C), and held for 15 min at this temperature to monitor the austenite-to-ferrite phase transformation. Finally, samples were quenched to room temperature at 60°C/s. The obtained Debye-Scherer diffraction rings, as illustrated in Fig.2-a, were converted to classical intensity-2 θ diffraction diagrams, as shown in Fig.2-b, by circular integration using the pyFAI software package [37]. Rietveld refinement

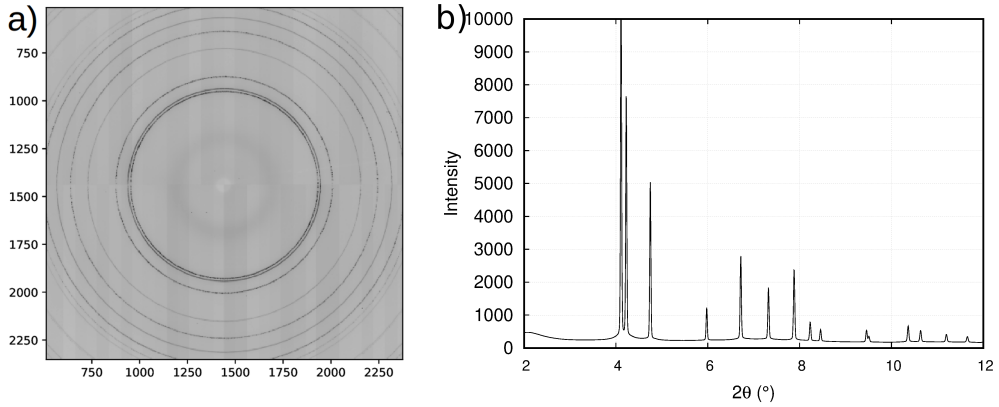

Figure 2: a) Debye-Scherer diffraction rings obtained from HEXRD experiments. b) Integrated 1D diffractogram (intensity vs 2θ).

was used to calculate phase fractions using the FullProf software package [38]. A pseudo-Voigt function was used to model the experimental diffraction peaks and a total of 18 parameters were used for Rietveld refinement, including scale and shape factors, temperature effect and lattice parameters.

3. Modeling

Experimental results were compared with the predicted ferrite growth kinetics using local equilibrium (LE), para-equilibrium (PE) and solute drag (SD) models. LE and PE calculations were carried out using the Thermo-Calc DICTRA software package, with the TCFE9 and MOB2 databases. Calculations were performed using an initial spherical parent grain. The initial grain size of austenite was measured by metallography techniques for each sample after the end of the partial transformation to ferrite, based on the assumption that ferrite nucleates at the boundary of austenite and grows into the spherical grain. An initial ferrite nucleus of thickness 100 nm was considered at the start of modeling, and thus nucleation was not taken into account.This initial condition is chosen as the nucleation happens exclusively intergranularly in the studied cases and is assumed to be complete in the first few seconds of the isothermal hold. As illustrated in Fig.3, ferrite (bright etched phase) is shown to nucleate on the whole austenite grain boundary indicating nucleation site saturation. Moreover, almost all the measured growth kinetics show some ferrite formation at time t=0. These data support the assumption that the effect of nucleation is significant only in the early stages of precipitation and that the overall transformation kinetics is mostly governed by the growth stage, save perhaps for the conditions where a more pronounced lag is observed. Thus, the effect of nucleation was ignored for analysis simplicity, as was the case in other ferrite precipitation studies [11, 39, 40, 41].

We developed a modified version of the three-jump solute drag model proposed by Zurob et al.[12] to predict the effect of composition and temperature on ferrite growth kinetics. In this model, the austenite-ferrite interface is considered as a thick interface comprising two discrete atomic layers. During ferrite growth, diffusion of substitutional

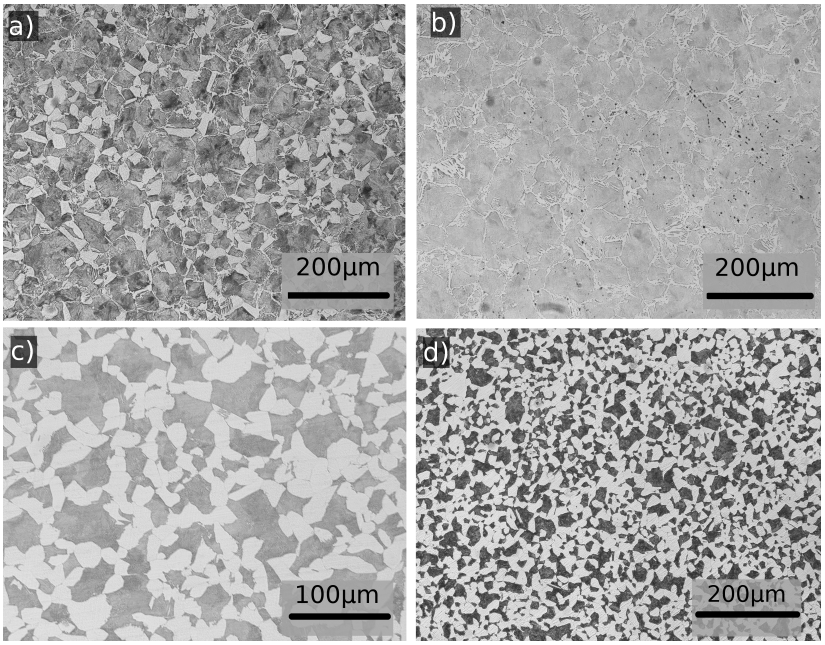

Figure 3: Micrographs showing microstructures of three samples : a) Fe-0.26C-0.3Mn, b) Fe-0.22C-1Ni, c) Fe-0.26C-1Cr and d) Fe-0.26C0.2Mo transformed at 750°C during 15 min. Ferrite is shown in bright and martensite in dark. The samples were etched using 4% metabisulfite (100 ml H_2O + 4 ml Na_2O_5)

elements across the interface involves three jumps across the interface, from ferrite to the first atomic layer, a second jump within the interface and a final jump to austenite. The solute diffusion across the interface results in a dissipated energy referred as the solute drag energy. The details of the different calculations in the three-jump model can be found in [12].

In this model, the thermodynamic properties of the interface are described using an approach developed by Hillert [12, 42]. The interface properties are modified from those of austenite by shifting the reference state for the free energy by 3.5 $kJ.mol^{-1}$. This value was chosen to capture an interfacial energy of 0.5 $J.m^{-2}$. In the present study, and in order to capture the significant segregation of carbon at the interface observed using atom probe experiments [25, 43], the interaction parameter between carbon and iron at the interface was adjusted from -34 $kJ.mol^{-1}$ (value in austenite) to -50 $kJ.mol^{-1}$ (see Fig.S6 and Fig.S7). This parameter is explained further in the text. A key feature of Zurob's model is the choice of two parameters: the binding energy of the substitutional element at the interface and the trans-interface diffusion coefficient of the solute element. These two parameters are not known experimentally, and generally used as fitting parameters. The binding energy (E_0) is generally defined as the difference between the chemical potential of solute X at the interface and the average chemical potentials of X in ferrite and austenite as shown in figure 4 [12, 44, 45]. ΔE is half the difference between the solute chemical potentials in austenite μ_X^γ and in ferrite μ_X^α. The binding energy parameter has been used to express the segregation behavior of the substitutional element at the interface [12, 14, 15, 45, 46, 47]. However, this parameter as calculated with this approach

depends on the conditions under which the calculations are made. The interface velocity and its associated carbon segregation affect the calculated binding energy significantly.

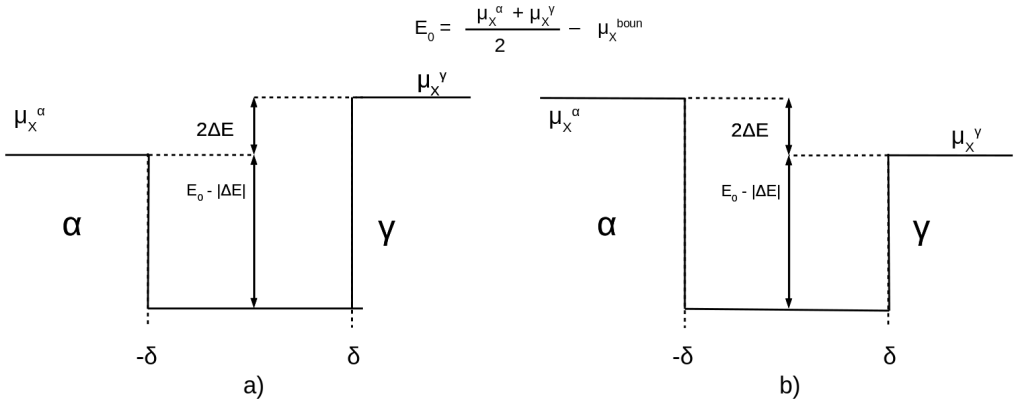

Figure 4: Schematic illustration of the potential well for (a) ferrite stabilizer and (b) austenite stabilizer inside the interface and the calculation of the binding energy in solute drag models.

The binding energies (E_0) predicted by solute drag models as shown in figure 4 have been compared to that obtained from APT measurements, which have been derived from the enrichment factor (K_{max}) [48, 25] using Eq.1, where $x_{X,max}$ and $x_{X,0}$ are the maximal X segregation at the interface and the bulk content, respectively. R and T are the gas constant and temperature, respectively.

$$K_{max} = \frac{x_{X,max}}{x_{X,0}} = \exp(\frac{E_0 - \Delta E}{RT}) \quad (1)$$

It should be noted that the effect of carbon co-segregation is not accounted for in the derivation of Eq.1. As a result, using Eq.1 to deduce the binding energy of an element from its segregation data returns a value that encompasses inter-elemental interactions. It may differ from the intrinsic binding energy of this element if the segregation data originates from multi-component systems.

In the present study, we propose to overcome this ambiguity, by evaluating the segregation behavior by means of an enrichment factor calculated at slow velocities (when equilibrium conditions are approached). To differentiate between the two calculated binding energies, shown in figure 4 and the one calculated using Eq.1, the latter will be called the effective binding energy (E_b).

In the present study, diffusion coefficients for the three jumps were chosen as the diffusion coefficient of element X in ferrite D_α for the jump from ferrite to the interface, the diffusion coefficient in austenite D_γ for the jump from the interface to austenite, and the geometrical average of D_α and D_γ for the jump within the interface. It is important to note that this choice of coefficients was retained for all studied systems. As a result, interfacial diffusion is not a fitting parameter as in previous studies [44]. The only fitting parameter remaining in the present study is the interaction parameter between Fe and substitutional element X at the interface. It must be emphasized that this parameter

does not express directly the segregation behavior of element X at the interface, which also depends on its interactions with the other elements of the system (carbon and other substitutional elements). For example, an element with a high affinity with carbon such as molybdenum will highly segregate at the interface due to the presence of carbon [27]. The interaction between Fe and element X is expressed using the ${}^{0}\mathrm{L}_{Fe,X:Va}$ thermodynamic parameter in the ThermoCalc database. The interaction parameter between carbon and iron is expressed using the ${}^{0}\mathrm{L}_{Fe:C,Va}$ thermodynamic parameter in the ThermoCalc database. Changing these parameters leads to a modification of the Wagner interaction parameter between X and C at the interface (ϵ_{XC}). In the present study, this value (ϵ_{XC}) was considered to have the same value as in austenite [20]. To this end, the Wagner interaction parameter was calculated both in austenite and at the interface and the difference was adjusted to obtain a similar value between the two parameters using Eq.2 [23].

$$\begin{aligned}\epsilon_{XC} = -\{\ ({}^{0}L_{Fe,X:Va} + {}^{1}L_{Fe,X:Va} + {}^{2}L_{Fe,X:Va}) + ({}^{0}L_{Fe:C,Va} - {}^{1}L_{Fe:C,Va} + \\ {}^{2}L_{Fe:C,Va}) - ({}^{0}L_{X:C,Va} - {}^{1}L_{X:C,Va} + {}^{2}L_{X:C,Va}) - ({}^{0}L_{Fe,X:C} + {}^{1}L_{Fe,X:C} \\ + {}^{2}L_{Fe,X:C}) - L_{Fe,X:C,Va}\ \}/RT\end{aligned} \tag{2}$$

In quaternary systems, the Wagner interaction between the two solutes X_1 and X_2 (ϵ_{X1X2}) at the interface is also affected by the fitting parameters (${}^{0}\mathrm{L}_{Fe,X1:Va}$ ${}^{0}\mathrm{L}_{Fe,X2:Va}$) interaction parameters. Again, the (ϵ_{X1X2}) interaction parameter in the interface is assumed similar to the one in austenite [20]. Once the ${}^{0}\mathrm{L}_{Fe,X1:Va}$ and ${}^{0}\mathrm{L}_{Fe,X2:Va}$ interaction parameters are adjusted, the Wagner interaction parameter between X_1 and X_2 (ϵ_{X1X2}) is calculated in both austenite and the interface and the difference is adjusted to capture the same ϵ_{X1X2} Wagner parameter as in austenite using Eq.3 [23].

$$\begin{aligned}\epsilon_{X1X2} = -\{\ ({}^{0}L_{Fe,X1:Va} + 2({}^{1}L_{Fe,X1:Va}) + 3({}^{2}L_{Fe,X1:Va})) + ({}^{0}L_{Fe,X2:Va} + \\ 2({}^{1}L_{Fe,X2:Va}) + 3({}^{2}L_{Fe,X2:Va})) - ({}^{0}L_{X1,X2:Va}) - (L_{Fe,X1,X2:Va})\ \}/RT\end{aligned} \tag{3}$$

To summarize, in the present study, the only used fitting parameter was the interaction between Fe and the substitutional element X at the interface expressed by the $\mathrm{L}_{Fe,X1:Va}$ parameter. The interaction parameter between iron and carbon at the interface was set to a constant value of -50 $kJ.mol^{-1}$ for the whole studied conditions (thus it was not used as a fitting parameter). Moreover, the interaction between X and C were also set to fixed values (equal to those in austenite) for the whole conditions, which makes them not fitting parameters. Finally, the diffusion coefficient at the interface was also set to a defined value (as the geometrical average of the two diffusion coefficients of carbon in austenite and ferrite) and thus not considered as a fitting parameter.

4. Results

4.1. Fe-C-Mn system

Three different manganese compositions (0.3, 0.7 and 1%wt.) were examined at three different temperatures 730°C, 750°C and 775°C. Figure S2 a, b and c show the isothermal sections of the Fe-C-Mn system calculated using the TCFE9 database of ThermoCalc,

at 730°C, 750°C and 775°C, respectively. At 730°C and 750 °C, the three studied compositions are located below the zero partition line, where both LENP and PE growth modes are expected. At 775°C, the 0.3%-Mn containing alloy (Fe-C-0.3Mn) is located below the zero partition line, Fe-C-0.7Mn lies on the zero partition line and Fe-C-1Mn is located above the LENP/LEP boundary.

The measured ferrite fractions as a function of time in the Fe-0.26C-0.3Mn, Fe-0.26C-0.7Mn and Fe-0.26C-1Mn systems are shown in figures 5 and 6, for the three temperatures 730°C, 750°C and 775°C. Table 2 summarizes the measured ferrite fractions at the end of the isothermal holding and the ones obtained using the different models as well as the measured grain sizes using metallography, for all the studied systems.

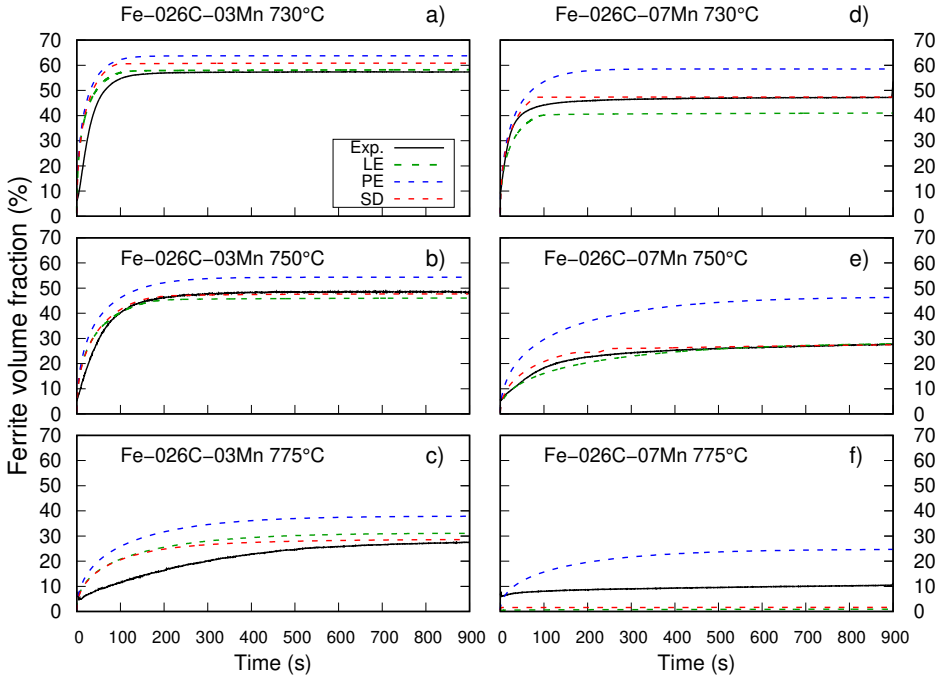

Figure 5: Comparison between the measured ferrite growth kinetics (solid black line) and the predictions of PE (dashed blue line), LE (dashed green line) and solute drag (dashed red line) models for the : a) Fe-0.26C-0.3Mn at 730°C, b) Fe-0.26C-0.3Mn at 750°C, c) Fe-0.26C-0.3Mn at 775°C, d) Fe-0.26C-0.7Mn at 730°C, e) Fe-0.26C-0.7Mn at 750°C and f) Fe-0.26C-0.7Mn at 775°C.

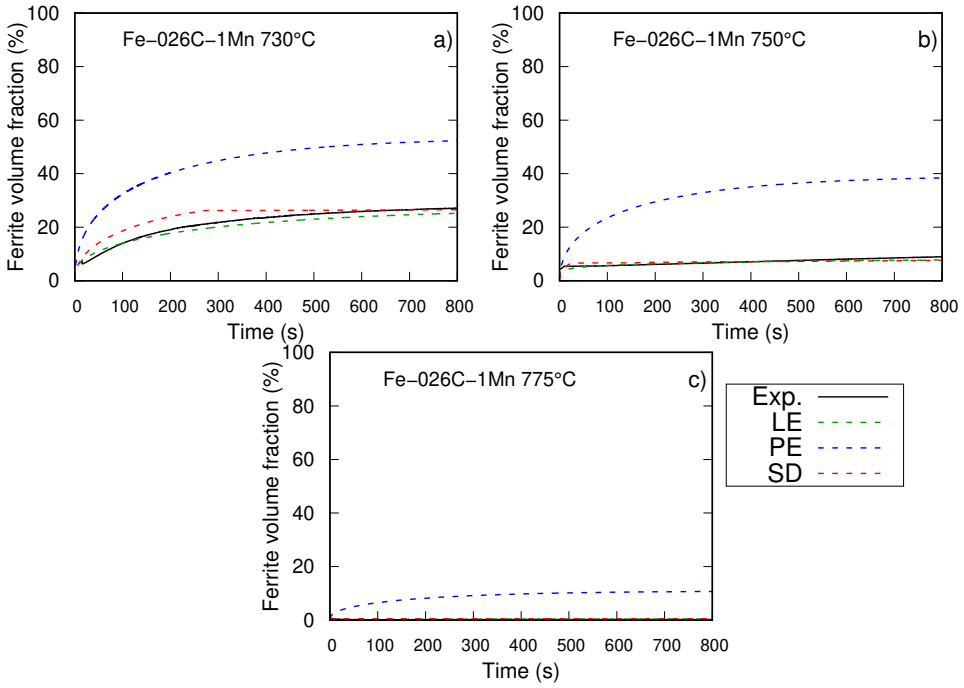

Figure 6: Comparison between the measured ferrite growth kinetics (solid black line) and the predictions of PE (dashed blue line), LE (dashed green line) and solute drag (dashed black line) models for the : a) Fe-0.26C-1Mn at 730°C, b) Fe-0.26C-1Mn at 750°C, c) Fe-0.26C-1Mn at 775°C.

For almost all the studied systems, the experimental ferrite growth tends toward a plateau where ferrite fraction is nearly constant. One can notice that for some cases, the volume fraction of ferrite at time 0 second starts from a non-zero value. This can be related to inaccuracy of ferrite measurements using Rietveld technique when ferrite fraction is below 5%, but also to nucleation starting during the transition from the austenitizing temperature to the transformation temperature, even though this transition was made to be as short as possible with the experimental setup. The measured growth kinetics as well as the final ferrite volume fraction reached at the plateau decrease with increasing temperature and manganese content. The predicted growth kinetics using the PE model is faster than the experimental measurements and the calculated ferrite fractions at the end of the transformation are overestimated by the PE model for all temperatures and manganese compositions. The LE predicted kinetics are slower than the PE calculated ones, and are for most Fe-C-Mn cases close to the experimental measured ones. For the 0.7-Mn containing system, one can notice that the measured kinetics at 730°C and 775°C lie between the PE and LE predicted ones. The solute drag model was also able to predict the measured ferrite growth kinetics at the three temperatures and for almost all the studied manganese compositions.

Table 2: Comparison between the measured final fraction (%) and the predicted ones using LE, PE and SD models for the Fe-C-Mn system.

Fe-C-Mn	T(°C)	f(Exp.)	f(LE)	f(PE)	f(SD)	Grain size(μm)
Fe-0.26C-0.3Mn	730	58	58	64	60	50 ($\pm$ 10)
Fe-0.26C-0.3Mn	750	49	47	55	48	80 ($\pm$ 16)
Fe-0.26C-0.3Mn	775	27	28	38	28	120 ($\pm$ 25)
Fe-0.26C-0.7Mn	730	47	41	59	47	120 ($\pm$ 25)
Fe-0.26C-0.7Mn	750	27	27	47	27	120 ($\pm$ 24)
Fe-0.26C-0.7Mn	775	10	0.5	25	2	120 ($\pm$ 24)
Fe-0.26C-1Mn	730	26	25	52	25	120 ($\pm$ 25)
Fe-0.26C-1Mn	750	9	8	38	8	120 ($\pm$ 30)
Fe-0.26C-1Mn	775	$<$2	1	13	1	120 ($\pm$ 28)
Fe-0.22C-1Ni	730	57	60	67	56	40 ($\pm$ 10)
Fe-0.22C-1Ni	750	40	44	53	41	40 ($\pm$ 12)
Fe-0.22C-1Ni	775	2	12	21	7	70 ($\pm$ 15)
Fe-0.26C-1Cr	750	48	52	55	48	120 ($\pm$ 25)
Fe-0.26C-1Cr	775	23	30	39	22	120 ($\pm$ 25)
Fe-0.26C-02Mo	730	62	65	65	62	50 ($\pm$ 10)
Fe-0.26C-02Mo	750	55	60	60	56	50 ($\pm$ 12)
Fe-0.26C-02Mo	775	40	46	46	40	60 ($\pm$ 15)

4.2. Fe-C-Ni system

The isothermal sections of the Fe-0.22C-1Ni (%.wt.) system at the three examined temperatures 730°C, 750°C and 775°C are shown in figure S3. The studied composition is located below the zero partition line for 730°C and 755°C temperatures, and on the partition boundary at 775°C.

The measured ferrite fractions as function of time for the Fe-C-Ni alloys are shown in figure 7 for the three temperatures 730°C, 750°C and 775°C, respectively. At 730°C and 750°C, the measured kinetics tends towards a plateau with a constant ferrite fraction. At 775°C, the growth kinetics is very slow and the final fraction at the end of the isothermal hold is (less than 1%). The comparison with the predicted ferrite growth kinetics using LE and PE models shows that the experimental results are slower than both modeled kinetics. The LE calculations predict closer final fractions at 730°C and 750°C. At 775°C, the measured ferrite fraction (2%) is much lower than the predicted one using LE calculations (12%) as well as the PE model (32%). The solute drag (SD) predicted kinetics are very close to the measured ones at both 730°C and 750°C and higher than the measured values at 775°C.

4.3. Fe-C-Cr and Fe-C-Mo systems

The measured ferrite growth kinetics for the Fe-C-Cr system is shown in figure 8 for the two temperatures 750°C and 775°C. The data obtained at 730°C are not shown here due to the formation of pearlite during the isothermal holding. At both temperatures, the measured ferrite growth kinetics are slower than those obtained using LE and PE models. The solute drag model predicts kinetics slower than both the PE and LE models and closer to the measured ones.

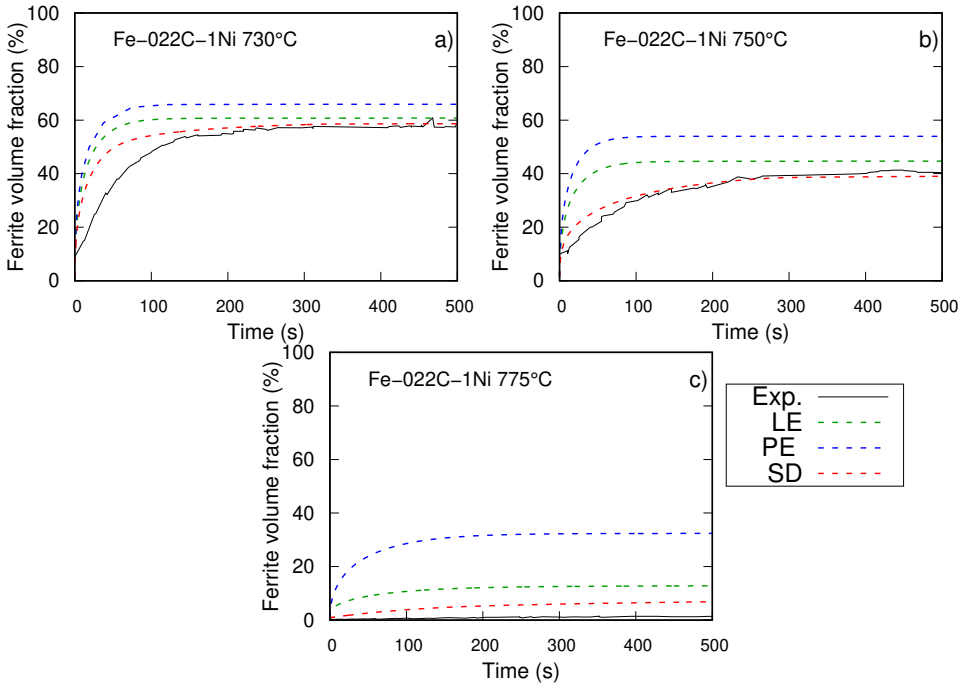

Figure 7: Comparison between the measured ferrite growth kinetics (solid black line) and the predictions of PE (dashed blue line), LE (dashed green line) and solute drag (dashed red line) models for the : a) Fe-0.22C-1Ni at 730°C, b) Fe-0.22C-1Ni at 750°C, c) Fe-0.22C-1Ni at 775°C.

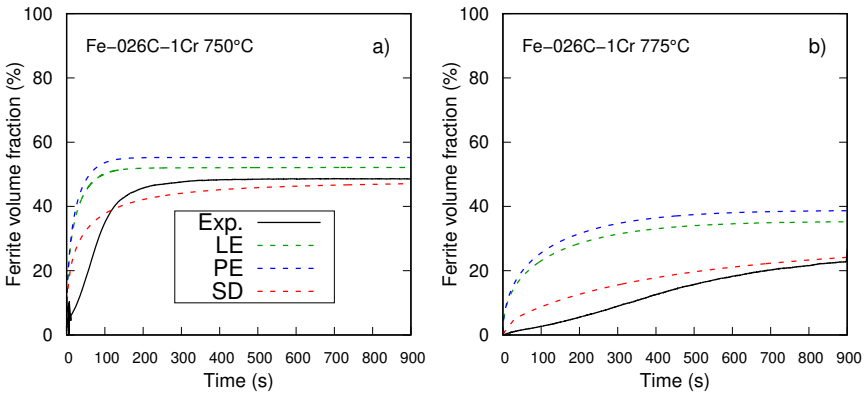

Figure 8: Comparison between the measured ferrite growth kinetics (solid black line) and the predictions of PE (dashed blue line), LE (dashed green line) and solute drag (dashed red line) models for the : a) Fe-0.26C-1Cr at 750°C, b) Fe-0.26C-1Cr at 775°C.

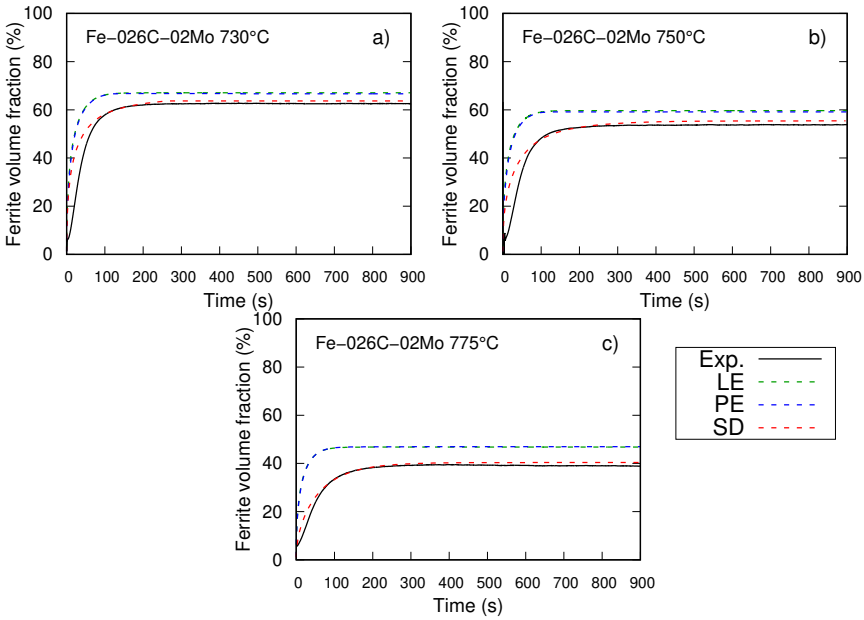

Figure 9: Comparison between the measured ferrite growth kinetics (solid black line) and the predictions of PE (dashed blue line), LE (dashed green line) and solute drag (dashed red line) models for the : a) Fe-0.26C-02Mo at 730°C, b) Fe-0.26C-02Mo at 750°C, c) Fe-0.26C-02Mo at 775°C.

Figure 9 shows the obtained ferrite fractions as function of time for the 0.2Mo containing system at the three temperatures 730°C, 750°C and 775°C, respectively. Under the chosen conditions, the predicted ferrite fractions using the PE and LE model are similar as shown in figure 9. Like the previous cases, ferrite fraction tends toward a plateau. For the three examined temperatures, the ferrite fractions at the plateaus are lower than the LE/PE predicted values (table 2). The SD predicted kinetics are slower than the LE/PE kinetics and agree well with the HEXRD measured kinetics.

4.4. Fe-C-Mn-Cr system

The measured ferrite fraction as a function of time for the quaternary Fe-0.26C-1Mn-1Cr system at 730°C is shown in figure 10. Ferrite fraction increases with time and tends towards a constant fraction (31%). The experimental kinetics lies between the LE and PE predicted ones and is well described by the SD model.

5. Discussion

5.1. Fe-C-Mn system

The solute drag (SD) model was applied to predict the measured ferrite growth kinetics in the Fe-C-Mn system as a function of composition and temperature. The predicted kinetics are plotted along with the measured ones as well as the LE and PE calculations in figures 5 and 6. In all cases except the 0.7wt.%-Mn alloy at 775°C,

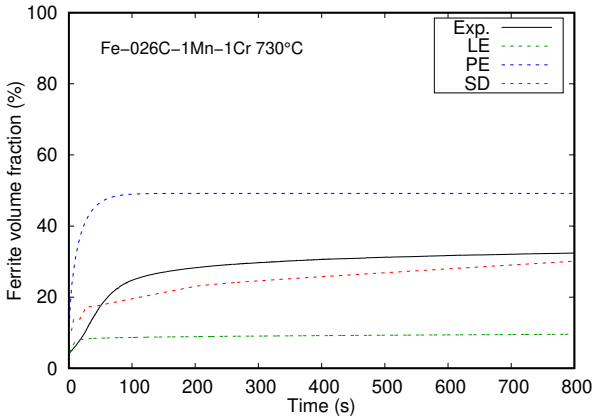

Figure 10: Comparison between the measured ferrite growth kinetics (solid black line) and the predictions of PE (dashed blue line), LE (dashed green line) and solute drag (dashed red line) models for the Fe-0.26C-1Mn-1Cr at 730°C.

excellent agreement was obtained between the SD model and the experiments. The SD model successfully predicts the measured kinetics in cases where both LE and PE fail to do so. It must be noted that two conditions (0.7wt.% and 1wt.% at 775°C) are located on and above the zero partition line where growth mode can be controlled by manganese diffusion in austenite (LEP mode). As mentioned before, the three-jump model considers that ferrite growth is always controlled by carbon diffusion only and the deviation from PE conditions is due to a dissipation of the available transformation energy by the diffusion of manganesein the interface. Thus, the model is not applicable when the partitioning of substitutional element is not negligible.

The Fe-Mn interactions parameters (${}^0L_{Fe,Mn:Va}$) used in the solute drag model to obtain the best fit of the experimental results are summarized in table 3. Results show a small decrease of the Fe-Mn interaction parameter with increasing temperature ($\Delta {}^0L_{Fe,Mn:Va}$: -0.5 $kJ.mol^{-1}$ when increasing temperature from 730°C to 775°C). However, the Fe-Mn interaction seems to be independent of composition (or at least this dependence is weak).

Table 3: The Fe-Mn interaction parameter ${}^0L_{Fe,Mn:Va}$ used in the solute drag modeling for the different Fe-C-Mn systems.

T(°C)	Fe-C-Mn	${}^0L_{Fe,Mn:Va}$ ($kJ.mol^{-1}$)	Fe-C-Mn	${}^0L_{Fe,Mn:Va}$ ($kJ.mol^{-1}$)	Fe-C-Mn	${}^0L_{Fe,Mn:Va}$ ($kJ.mol^{-1}$)
730	0.3Mn	-1.4	0.7Mn	-1.5	1Mn	-1.5
750	0.3Mn	-1.6	0.7Mn	-1.8	1Mn	-1.8
775	0.3Mn	-1.9	0.7Mn	-2.0	1Mn	-2.0

Zurob et al.[12] investigated the ferrite growth kinetics using decarburization experiments in Fe-C-Mn systems and reported a binding energy of -2.5 $kJ.mol^{-1}$ to model the observed kinetics. The binding energy was calculated under PE conditions (i.e. at high interface velocity). Using the same calculation conditions, the obtained binding energy in the

present study is +1.5 $kJ.mol^{-1}$ for all the studied manganese compositions and at the three temperatures. In both Zurob's modeling and the present one, only the Fe-Mn interaction parameter was used as a fitting parameter. The difference between the two obtained binding energies (+1.5 $kJ.mol^{-1}$ and -2.5 $kJ.mol^{-1}$) can be attributed to the difference in the thermodynamic properties of the interface as used by Zurob et al.[12] and in the present study. The carbon-iron interaction parameter (expressed using the ${}^0L_{Fe:C,Va}$ parameter of ThermoCalc database) used by Zurob [12] was -34 $kJ.mol^{-1}$ (as in austenite) versus a value of -50 $kJ.mol^{-1}$ in the present study. Moreover, in the present version of the model, the interaction between manganese and carbon (ϵ_{XC}) was modified to capture a similar value as in austenite. As already mentioned, modifying the Fe-Mn (${}^0L_{Fe,Mn:Va}$) and Fe-C (${}^0L_{Fe:C,Va}$) interaction parameters results in a change of the Wagner interaction parameter between manganese and carbon at the interface (ϵ_{MnC}). In this study this parameter was re-adjusted to a similar value as in austenite. In Zurob's model[12], this parameter was not re-adjusted meaning that the Wagner interaction parameter (ϵ_{MnC}) can be different from that in austenite.

In the following section, the effect of these two changes (Fe-C (${}^0L_{Fe:C,Va}$) and X-C (ϵ_{MnC}) interaction parameters) on the solute segregation behavior is detailed. To this end, three cases representing the different modifications are studied. In the first case, no changes were made to either the Fe-C or the X-C interaction parameters. This approach is similar to the one used by Zurob et al.[12]. In the second case, the Fe-C interaction parameter (${}^0L_{Fe:C,Va}$) at the interface is modified to -50 $kJ.mol^{-1}$ but the X-C interaction parameter (ϵ_{MnC}) is not re-adjusted to a similar value as that in austenite. Finally, the last case represents the current configuration of the model, where the Fe-C (${}^0L_{Fe:C,Va}$) interaction parameter is modified to -50 $kJ.mol^{-1}$ and the X-C interaction parameter (ϵ_{MnC}) is re-adjusted to the austenite value. In all three cases, the Fe-Mn (${}^0L_{Fe,X:Va}$) interaction parameter (and thus the binding energy) was modified to obtain the best fit of the experimental data.

Table 4: The binding energies, E_0 ($kJ.mol^{-1}$) used to obtain the best fit of the experimental growth kinetics using the three different approaches for the Fe-C-Mn system. Approach 1 : ${}^0L_{Fe:C,Va}$:-34 $kJ.mol^{-1}$, ϵ_{MnC} : not re-ajusted. Approach 2 : ${}^0L_{Fe:C,Va}$:-50 $kJ.mol^{-1}$, ϵ_{MnC} : not re-ajusted. Approach 3 : ${}^0L_{Fe:C,Va}$:-50 $kJ.mol^{-1}$, ϵ_{MnC} : ϵ_{MnC} in austenite.

Fe-0.26C-xMn	T(°C)	E_0 Approach 1	E_0 Approach 2	E_0 Approach 3
0.3Mn	730	-1.5	-1.5	+1.5
0.3Mn	750	-1.5	-1.5	+1.5
0.3Mn	775	-1.5	-1.5	+1.5
0.7Mn	730	-1.5	+0.5	+1.5
0.7Mn	750	-1.5	+0.5	+1.5
0.7Mn	775	-1.5	/	/
1Mn	730	+0.5	+1.5	+1.5
1Mn	750	+0.5	+1.5	+1.5
1Mn	775	+0.5	+1.5	+1.5

Table 4 summarizes the calculated binding energies that yielded the best fit of the experimental data for the Fe-C-Mn using the three approaches. One can notice that the

binding energy required to get the best fit of the experimental data changes when other thermodynamic parameters of the interface are modified.

Figure 11 shows the evolution of the total dissipated energy and the dissipation due to manganese transfer at each atomic plane, as a function of velocity for the Fe-C-1Mn alloy at 730°C using the 3 different approaches used to model the experimental growth kinetics. The total dissipated energies are comparable for the three cases, with a maximum of 45 $J.mol^{-1}$ attained at medium velocities ($1e^{-7}$ to $1e^{-9}$ m/s). At high velocities, the dissipated energy is mostly due to the diffusion of manganese from ferrite to the first interfacial atomic plane (the first jump, named flux J1). It can be seen from Fig.11 that this dissipated energy (SD1) depends on the used approach.

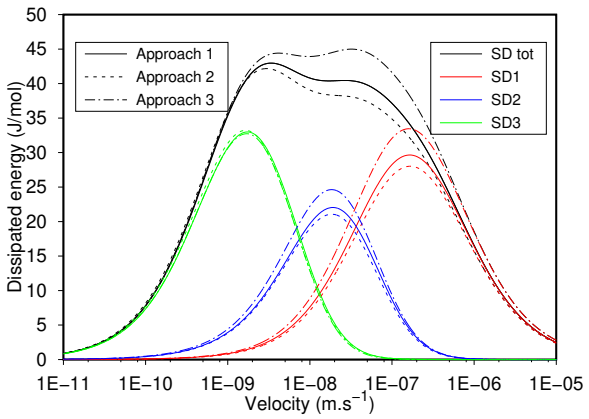

Figure 11: The dissipated free energy due to Mn diffusion across the interface (at each jump) as function of the interface velocity for the Fe-0.26C-1Mn at 730°C calculated using the three approaches to describe the interaction parameters at the interface. Approach 1 : Fe-C : -34 $kJ.mol^{-1}$, Mn-C : not re-adjusted. Approach 2 : Fe-C : -50 $kJ.mol^{-1}$, Mn-C : not re-adjusted. Approach 3 : Fe-C : -50 $kJ.mol^{-1}$, Mn-C : as in austenite.

With decreasing velocity, the dissipated energy, SD2, due to manganese diffusion within the interface starts to increase. The maximum dissipated energy SD2 follows the same trend as SD1. At low velocities, the total dissipated energy is mostly due to the flux of Mn atoms from the second interfacial atomic plane to the austenite interface side. The maximum dissipated energy due to this flux (J3) is independent of the used approach.

The effect of the approach used to describe the interaction parameters at the interface is more noticeable when comparing the solute segregation at the different interfacial atomic layers. The evolution of manganese contents at the different atomic planes as well as the carbon content at the austenite interface side are plotted as function of velocity in figure 12. The carbon content on the austenite side of the interface increases with increasing interface velocity and its evolution is comparable for the three approaches. When no modifications are made to the Fe-C and Mn-C interaction parameters (Fig.12-a), the segregation of Mn at the interface (Mn1 and Mn2) reaches a maximum of 340% of the the bulk composition (K_{max}= 3.4) at low interface velocities (< $1e^{-9}$ m.s^{-1}). The Mn content at the austenite interface reaches a maximum of 310% at low velocities. When changing the Fe-C interaction parameter ($^0L_{Fe:C,Va}$) to -50 $kJ.mol^{-1}$ (Fig.12-b), the maximum of Mn segregation at the two atomic planes decreases to 270%. This

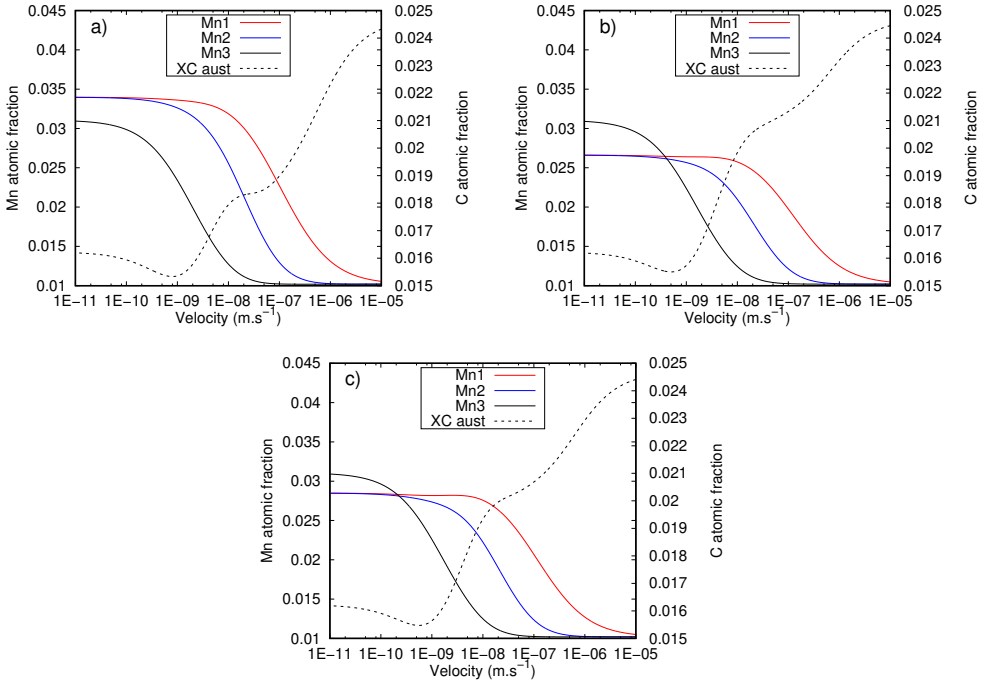

Figure 12: Evolution of Mn content at the different atomic planes (1, 2 and 3) of the interface as well as the carbon content at the austenite interface side as function of interface velocity for the Fe-0.26C-1Mn at 730°C calculated using the three approaches to describe the interaction parameters at the interface. a) Fe-C : -34 $kJ.mol^{-1}$, Mn-C : not re-adjusted. b) Fe-C : -50 $kJ.mol^{-1}$, Mn-C : not re-adjusted. c) Fe-C : -50 $kJ.mol^{-1}$, Mn-C : as in austenite.

can be explained by the higher content of carbon present at the interface when using a Fe-C interaction of -50 $kJ.mol^{-1}$. As a result, less manganese is needed to obtain the same ferrite growth kinetics (the same carbon evolution at the austenite interface side). Moreover, setting the Fe-C interaction parameter to -50 $kJ.mol^{-1}$ induces a change in the Mn-C interaction parameter (ϵ_{XC}) and results in a less attractive value between Mn and C at the interface compared to austenite.

When re-adjusting the Mn-C Wagner interaction parameter (ϵ_{XC}) at the interface to a similar value as in austenite (Fig.12-c), the maximum of Mn segregation at the interface increases to 290% of the bulk composition (K_{max}= 2.9). As stated before, the Mn-C interaction parameter is dependent on the Fe-Mn and Fe-C interaction parameters at the interface. By taking into account this effect, the new interaction between Mn-C is more attractive compared to the case where only the Fe-C interaction parameter was changed. As a result, the required Mn content at the interface in order to obtain the same ferrite growth kinetics is lower than the former case (only the Fe-C interaction parameter is changed).

5.2. Fe-C-Ni system

The solute drag model was also applied to the Fe-C-Ni system at the three temperatures 730°C, 750°C and 775°C. As in the Fe-C-Mn system, the interaction parameter between iron and carbon at the interface (${}^0L_{Fe:C,Va}$) was set to -50 $kJ.mol^{-1}$ and the Wagner interaction parameter between nickel and carbon (ϵ_{NiC}) at the interface was modified to capture the same value as in austenite. The interaction parameter between nickel and iron at the interface was used as the only fitting parameter. Using this set of parameters, good agreement between the experimental results and the predicted kinetics were obtained at 730°C and 750°C as shown in Fig.7. For the 775°C temperature, the predicted growth kinetics is faster than the measured one. The Fe-Ni interaction parameter that gave the best fit of the experimental data is -11.7 $kJ.mol^{-1}$ at 730°C, -11.8 $kJ.mol^{-1}$ at 750°C and -11.9 $kJ.mol^{-1}$ at 775°C corresponding to a binding energy of -6.5 $kJ.mol^{-1}$ for the three temperatures, when calculated under para-equilibrium conditions. Qiu et al. [14] used a binding energy (calculated under the same conditions) of +1.5 $kJ.mol^{-1}$ for predicting ferrite growth kinetics in Fe-C-Ni alloys. Oi et al. [6] on the other hand reported a nickel binding energy calculated under the same conditions of -4 $kJ.mol^{-1}$.

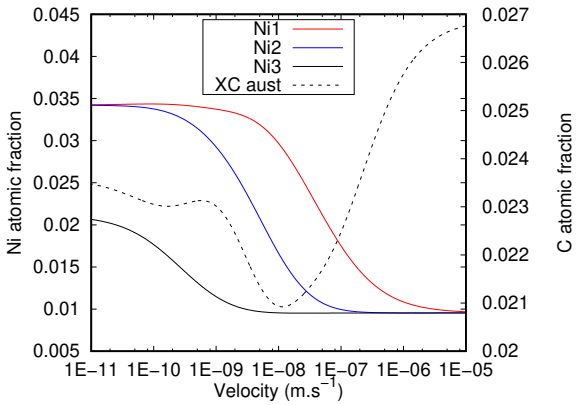

Figure 13: Evolution of Ni content at the different atomic planes of the interface as well as the carbon content at the austenite interface side as function of interface velocity for the Fe-0.22C-1Ni at 730°C.

An example of the dissipated energy as function of velocity for the Fe-C-Ni alloy at 730°C is shown on figure S4 . The evolution of nickel segregation at different atomic planes as well as the interfacial carbon content as function of interface velocity are illustrated in figure 5.2. It can be noticed that the transformation energy is mostly dissipated by diffusion of nickel from ferrite to the first atomic plane and from the first atomic plane to the second one. The maximal dissipated energy (63 $J.mol^{-1}$) is reached at $1e^{-8}$ $m.s^{-1}$. The maximum segregation of nickel at the interface (atomic planes 1 and 2) is 360% (K_{max} = 3.6) compared to the bulk composition and 1.6 times higher than the nickel segregation at the austenite interface side which represents the LENP spike. When increasing the temperature to 750°C, the maximal dissipated energy increases to 65 $J.mol^{-1}$ and the enrichment factor of nickel (K_{max}) at the interface to 3.7. At 775°C the maximum dissipated energy is 80 $J.mol^{-1}$ and the nickel segregation is 380% compared to the bulk composition (K_{max} = 3.8). Although the highest dissipated energy

is obtained at 775°C, the predicted kinetics is faster than the HEXRD measurements. It is interesting to notice that this condition (1wt.% at 775°C) is located on the zero partition line. The very low measured ferrite fraction indicates that the transformation is controlled by nickel diffusion in austenite i.e. under LEP conditions. Again, the present model is not applicable under such conditions.

5.3. Fe-C-Mo and Fe-C-Cr systems

Both molybdenum and chromium are ferrite-stabilizing elements and hence it is interesting to compare ferrite growth in these systems with that obtained in systems containing austenite stabilizers such as nickel and manganese. Moreover, chromium and molybdenum are known to have a strong interaction with the interface when compared to that of nickel and manganese [27, 19].

The measured ferrite growth kinetics in the Fe-C-Mo system showed slower kinetics than those predicted by both PE and LE, meaning that the observed experimental deviation from both models is due to an additional dissipated energy during the phase transformation. Moreover, at the chosen composition and temperatures, both LE and PE predicted similar kinetics. This is attributed to the fact that under these conditions, the chemical potentials of molybdenum in austenite and ferrite are almost the same. The predicted kinetics using the solute drag model are in good agreement with the experimental ones at all three temperatures, indicating that the additional dissipated energy can be attributed to molybdenum diffusion across the interface. The best fit of the experimental results was obtained using a Fe-Mo interaction parameter of -7.1 $kJ.mol^{-1}$, -7.5 $kJ.mol^{-1}$ and -7.9 $kJ.mol^{-1}$ corresponding to a binding energy of -15 $kJ.mol^{-1}$ for the three temperatures as calculated under para-equilibrium conditions. Zurob et al. [12] reported the same binding energy calculated under the same conditions to model ferrite growth kinetics in a Fe-0.51Mo-0.54C (%wt.) alloy at 806°C and 825°C.

Hutchinson et al. [27] measured the ferrite growth kinetics in a Fe-0.54C-0.51Mo (%wt) steel at 775°C using decarburization experiments. The authors reported a deviation from the LENP/PE model predictions and attributed this difference to an additional energy dissipation due to solute drag effect. The estimated dissipated energy needed to shift the LENP/PE kinetics to the measured ones was 43 $J.mol^{-1}$. The authors reported that the magnitude of this energy decreases with increasing temperature. In the present study, the same trend was observed concerning the maximal dissipated energy as function of temperature, 84 $J.mol^{-1}$, 70 $J.mol^{-1}$ and 56 $J.mol^{-1}$ at 730°C, 750°C and 775°C, respectively.

Figure S5-a shows an example of the dissipated energies due to molybdenum diffusion across the interface as function of velocity for the 730°C temperature. The corresponding evolution of molybdenum segregation at the interface as well as carbon interfacial content as a function of interface velocity is plotted in figure 14-a. It can be noticed that the total dissipated energy is mostly due to molybdenum diffusion across the interface and that the molybdenum spike (third plane) has a small effect on the dissipated energy. The maximum dissipated energy decreases with increasing temperature as well as the molybdenum segregation at the interface.

The experimental results obtained for the Fe-0.26C-1Cr system at 750°C and 775°C were finally compared with the predictions of the different models. Both PE and LE predicted kinetics are slower than the experimental observations indicating an extra dissipation of energy due to solute drag. The Fe-Cr interaction parameter was modified

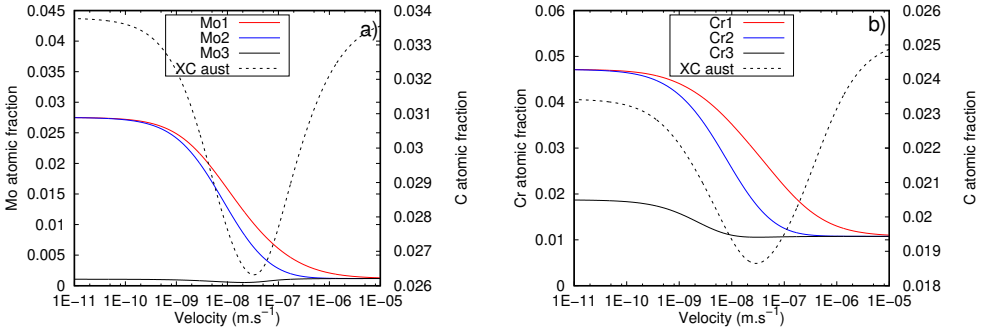

Figure 14: The evolution of Mo (a) and Cr (b) content at the different atomic planes of the interface as well as the carbon content at the austenite interface side as function of interface velocity for Fe-0.26C-0.2Mo at 730°C and Fe-0.26C-1Cr at 750°C, respectively.

to fit the experimental kinetics. The best fit was obtained using an Fe-Cr interaction parameter of +5.1 $kJ.mol^{-1}$ at 750° C and +4.9 $kJ.mol^{-1}$ at 775°C, corresponding to a binding energy calculated under para-equilibrium conditions of +1.5 $kJ.mol^{-1}$ and -1.5 $kJ.mol^{-1}$, respectively. Panahi et al. [49] used the solute drag model to predict ferrite growth kinetics in a Fe-0.58C-2Cr (%wt.) alloy at different temperatures (775 °C to 850°C) and reported a binding energy of -1.5 $kJ.mol^{-1}$ as calculated under para-equilibrium conditions. Results show a temperature dependence of the Cr binding energy which was not observed in other systems. Given the small magnitude of this dependence, one should not draw definitive conclusions about chromium segregation behaviour from these two experimental results. It is clear however, that this observation should be investigated more deeply using additional experimental conditions.

The dissipated energies as a function of velocity are shown in figure S5-b for the 750°C case. The corresponding segregation behavior of molybdenum at the interface is shown in figure 14-b. As for the Fe-C-Mo system, the dissipation due to solute diffusion across the interface contributes the most to the total dissipated energy. In contrast to the previous observation in the Fe-C-Mo system, a similar dissipated energy is observed at higher temperatures. At 750°C, the maximal dissipated energy is 68 $J.mol^{-1}$, as is the case at 775°C. Béché et al. [26] estimated the dissipated energy necessary to bring the PE model in agreement with the observed kinetics in a Fe-0.58C-2Cr (wt.%) steel. At 775°C, the authors reported a dissipated energy of 50 $J.mol^{-1}$.

5.4. The segregation behavior of the different substitutional elements

As stated above, comparing the binding energies as calculated under para-equilibrium conditions to express the segregation behavior of the element to the interface can be misleading.

This issue can explain the discrepancy between the binding energies that can be found in the literature for the same element. Zurob et al.[12] and Chen et al.[45] both studied ferrite growth kinetics in the Fe-C-Mn system using solute drag based models. The binding energy of manganese was reported to be around -2.5 $kJ.mol^{-1}$ in Zurob's calculations [12] and -9.9 $kJ.mol^{-1}$ in Chen's [45] study. However, when comparing the enrichment factors of manganese (K_{max}), from the two models, similar values are found,

3.3 at 755°C in Zurob's study and 3.4 at the same temperature in Chen's study. This difference in the calculated binding energies can originate from the considered conditions in the calculations. In Zurob's [12] approach, the binding energy is calculated at the initial PE conditions, i.e. high interface velocity and no carbon segregation. This value can be highly different from the calculated one at the local equilibrium conditions. In Chen's approach, it is not clear under which conditions the binding energy was calculated.

For a better understanding of the segregation behavior of solute elements at the interface, one should compare the segregation profiles. In Zurob's study [14], the manganese enrichment factor (K_{max}) calculated at 775°C for a Fe-0.57C-0.94Mn (%wt.) steel composition is 3.1. At the same temperature, the manganese enrichment factor obtained by the present modeling for the Fe-C-1Mn alloy is 2.17. Van Landeghem et al. [43] used atom probe tomography (APT) to study solute segregation at the austenite/ferrite interface in Fe-C-X alloys. The authors reported an enrichment factor of 2.47 for a Fe-0.57C-0.94Mn (%wt.) alloy transformed at 775°C. One has to note that the interface width obtained in Van Landeghem et al.'s [43] study is 3 nm compared to 1 nm in the present model. As a result, the enrichment factor as calculated by Van Landeghem et al. can be higher if a 1 nm interface width is considered. Danoix et al.[25] measured the segregation of manganese at the austenite ferrite interface of a Fe0.12C-2Mn (wt.%) alloy at 680°C obtained by precipitation experiment. In their study, Danoix et al. found an interface width of 1 nm, similar to that considered in the present study. The authors reported an enrichment factor of manganese of 3.7 at 680°C. Using the expression of the enrichment factor as function of the effective binding energy and temperature (Eq.1) and assuming that the effective binding energy is independent on temperature, the K_{max} estimated at 775°C is 3.2. The obtained enrichment factor in the present study (2.17) is slightly lower but comparable to the measured ones (2.47 and 3.2). The difference could be explained by joint effects of carbon content and temperature. Elucidating this effect would require data points with varying carbon contents at the same transformation temperature and same manganese composition.

As it was shown in figure 5.2-b, the predicted segregation values of nickel at the interface are surprising since the reported APT measurements on the Fe-C-Ni system show no segregation or very low segregation of nickel at the interface [43]. Qiu et al. [14] studied ferrite growth kinetics in a Fe-0.74C-1.46Ni (wt. %) alloy and reported a K_{max} of 2.4 at 755°C. It has to be noted that the authors used a binding energy of $+2.5\ kJ.mol^{-1}$ (as calculated under para-equilibrium conditions). This again shows that calculating the binding energy under these conditions is not representative of the segregation tendency of an element.

The predicted enrichment factors for molybdenum at the interface were 20, 18 and 14.5 at the temperatures 730°C, 750°C and 775°C, respectively. The reported APT measurements conducted by Van Landeghem et al.[43] on the Fe-0.57C-0.5Mo (wt.%) system at 806°C showed a K_{max} of 8.48 corresponding (Eq.1) to a K_{max} of 9 at 775°C. The experimental value is thus lower than the value predicted by the present modeling (14.5). One possible cause of this difference can emerge from the interface thickness in the APT measurements (3 nm) and the assumed one in the SD model (1 nm). Using the reported effective binding energy by Van Landeghem et al.[43] for the same alloy considering a 1 nm interface width, the adjusted K_{max} from APT results is 12.5 compared to 14.5 in the present study.

The chromium enrichment factor was 4.3 for both temperatures 750°C and 775°C,

respectively. The K_{max} value reported by Van Landeghem et al. [43] using APT measurements is 2.7 for a Fe-0.57C-2Cr (%wt.) at 806°C corresponding to 2.9 for 775°C. This value is lower than the predicted one using the present model, namely 4.3. However, if one considers the effect of the interface thickness, the new experimental K_{max} estimated in Van Landeghem's [43] study is 5.3, which is comparable to the predicted value in the present work (4.3).

5.5. The intrinsic segregation energy

Danoix et al. [25] estimated an effective binding energy of manganese of -6 $kJ.mol^{-1}$ using the formula in Eq.1. Using the same approach, the effective binding energy calculated for the Fe-C-1Mn at 730°C in the present study is -5 $kJ.mol^{-1}$ with ΔE as -4.4 $kJ.mol^{-1}$ calculated using TCFE9 database of ThermoCalc. This value is comparable with the reported segregation energies of manganese on austenite grain boundaries (-8 (+/- 3) $kJ.mol^{-1}$ [20]) or at ferrite grain boundaries [50] (-5.5 $kJ.mol^{-1}$). However, the reported values represent the intrinsic segregation energies (intrinsic binding energies) of manganese. As it was mentioned, the effective binding energy as calculated using Eq.1 does not take into account the effect of other segregated elements at the interface such as carbon in the present case.

Qiu et al. [14] reported an effective segregation energy of -4 $kJ.mol^{-1}$ calculated using Eq.1 for nickel in a Fe-0.74C-1.46Ni (wt. %) alloy at 755°C. The calculated effective segregation energy using Eq.1 of the Fe-C-1Ni at 730°C is -7.5 $kJ.mol^{-1}$ with a ΔE of -3.4 $kJ.mol^{-1}$ calculated using TCFE9 database of ThermoCalc. The difference between the present value and the one estimated by Qiu et al. (-4 $kJ.mol^{-1}$) is partially due to the carbon segregation at the interface, which is enhanced in the present study due to the modification of the interaction parameter between carbon and iron at the interface.

Finally, for molybdenum and chromium, the estimated effective segregation energies using equation 1 are -25 $kJ.mol^{-1}$ at 730°C for molybdenum and -12 $J.mol^{-1}$ at 750°C for chromium. Again, the effective segregation energies as calculated using Eq.1 are not representative of the intrinsic segregation energy of the element X.

To estimate the intrinsic segregation energy, the effect of carbon can be decorrelated using Guttmann's approach [50, 20] of grain boundary segregation in interacting multi-component systems. The intrinsic segregation of an element X (ΔG^0_X) in a Fe-C-X system where X is a substitutional element and C is an interstitial element (carbon) is estimated using Eq 4.

$$\Delta G^0_X = \Delta G_X + 2\beta_{FeX}(Y^{boun}_X - Y^B_X) - \beta_{XC}(Y^{boun}_C - Y^B_C) \tag{4}$$

where $Y^{boun}_X = \frac{x^{boun}_X}{1-x^{boun}_X}$, $Y^B_X = \frac{x^B_X}{1-x^B_X}$, B is the bulk phase, *boun* is the boundary phase and ΔG_X is the effective segregation energy (similar to E_0 in Eq.1) estimated at equilibrium between the bulk (B) and the boundary (boun) ($\mu^{boun}_X = \mu^B_X$) as follows :

$$\frac{Y^{boun}_X}{1-Y^{boun}_X} = \frac{Y^B_X}{1-Y^B_X}\exp(-\frac{\Delta G_X - \Delta E}{RT}) \tag{5}$$

β_{FeX} and β_{XC} are the interaction parameters of Fe with X and X with C, assumed to be similar in the bulk phase and at the interface and their values are summarized in table

5. The β_{FeX} interaction parameter was estimated using the L interaction parameters of the two-sublattice model as :

$$\beta_{FeX} = {}^{0}L_{Fe,X:Va} + {}^{1}L_{Fe,X:Va}(1 - 4Y_X) \quad (6)$$

β_{XC} represent the interaction between substitutional elements and carbon and its value can be calculated using :

$$\beta_{XC} = {}^{o}G_{Fe} + {}^{o}G_{XC} - {}^{o}G_{FeC} - {}^{o}G_X \quad (7)$$

${}^{o}G_{Fe}$ and ${}^{o}G_X$ are the standard free energy of pure Fe and pure X, respectively. ${}^{o}G_{XC}$ and ${}^{o}G_{FeC}$ are the Gibbs free energies of hypothetical compounds where all of the interstitial sites are filled with carbon and all the substitutional sites are filled with elements X and iron, respectively. The values of β_{XC} were extracted from [51].

Table 5: Numerical values of β_{FeX} and β_{XC} coefficients in Fe-C-X used in austenite and the boundary phase

X	β_{FeX} $J.mol^{-1}$	β_{XC} $J.mol^{-1}$ [51]
Mn	-7762+3.865×T - (1 - 4 × Y_X)×259	-48500
Ni	-12054.355+3.27413×T	46000
Mo	28347-17.691×T	-89080
Cr	10833-7.477×T +1410 ×(1 - 4× Y_X)	-251160 + 118×T

However, to apply this approach in the present case, a hypothesis must be made on the nature of the bulk phase. In the following procedure, the bulk phase is considered as austenite. Moreover, in Guttmann's approach, the boundary phase is considered to have the same thermodynamic properties as the bulk with the difference that the standard chemical potentials of Fe and X are shifted by σ_1A and σ_2A, respectively, where σ_1 and σ_2 are the grain boundary energies of pure Fe and elements X and A is the molar area of atoms at the interface. Using this approach, the intrinsic segregation energy of the element X can simply be estimated as ($\Delta G^0_X = \sigma_1 A - \sigma_2 A$).

Here again, the present model uses a different approach, where the segregation of the elements are expressed by modifying the Fe-X interaction parameter of the interface and the $\sigma_1 A$ and $\sigma_2 A$ are set to +3500 $J.mol^{-1}$ for iron and all substitutional elements. However, Guttmann's approach can be used as an analogy in the present case, meaning that the results of the present model (the segregation contents) are used to calculate the segregation energy using Eq.5 and then the intrinsic segregation energy of the element X is estimated using Eq.4 assuming a thermodynamic approach of the interface similar to Guttmann's.

Using this approach, the calculated intrinsic segregation energy of the different elements are summarized in table 6.

The solute drag modeling shows that segregation of manganese at the α/γ interface is increased due to the presence of carbon (effective segregation of -5 $kJ.mol^{-1}$) and that its intrinsic segregation (-2.2 $kJ.mol^{-1}$) is weak to such interfaces. Van Landeghem et al. [24] used APT to measure manganese segregation at the austenite ferrite interface in Fe-C-Mn and Fe-N-Mn alloys. Manganese has an attractive interaction with both carbon and nitrogen in austenite and ferrite. It was reported that nitrogen, in contrast

Table 6: Numerical values of β_{FeX} and β_{XC} coefficients in Fe-C-X used in austenite and the boundary phase

Element	ΔG^0 ($kJ.mol^{-1}$)	ΔG^0 ($kJ.mol^{-1}$) in austenite grain boundaries	ΔG^0 ($kJ.mol^{-1}$) in ferrite grain boundaries
Mn	-2.2	-8 ($\pm$3) [20]	-5.5 [50]
Ni	-9.5	$>$ -7 [20]	-3 ($\pm$3) [50]
Mo	-14.5	-15 ($\pm$3) [20]	0.1 [50], -28 [52]
Cr	-1.9	-10 [20]	0 [50]

to carbon, segregates little at grain boundaries. Van Landeghem et al.[24] reported a significant segregation of manganese at the austenite ferrite interface in the Fe-C-Mn and a weak or nonexistent segregation in the Fe-N-Mn system. These observations suggest that the presence of carbon at the austenite ferrite interface is the main factor responsible for manganese segregation at the austenite and ferrite. This is in agreement with the calculations made in the present study.

For nickel, the intrinsic segregation energy calculated in the present study indicates a higher tendency for nickel to segregate to the austenite-ferrite interface, contrary to the reported low segregation of this element to such interfaces [14] or at grain boundaries [20, 50].

The intrinsic segregation energy of molybdenum is in good agreement with the reported value in austenite grain boundaries [20]. On the other hand, Guttmann et al. [50] estimated a very low binding energy of molybdenum at ferrite grain boundaries (0.1 $kJ.mol^{-1}$) and claimed that the observed molybdenum segregation is only due to carbon presence at the interface. However, Murayama et al. [52] showed that molybdenum can segregate at α-Fe grain boundaries and estimated an intrinsic segregation energy of -28 $kJ.mol^{-1}$ at 800°C. For chromium, calculations show that the presence of chromium at the interface is mainly due to its attractive interaction with carbon. This is in good agreement with the reported intrinsic segregation energy of chromium at ferrite grain boundaries [50]. On the other hand, Enomoto et al.[20] estimated an intrinsic segregation energy of chromium at austenite grain boundaries of -10 $kJ.mol^{-1}$.

5.6. Fe-C-Mn-Cr system

The quaternary version of the solute drag model was used to predict the ferrite growth kinetics in the Fe-0.26C-1Mn-1Cr system at 730°C. To this end, the same Fe-Mn and Fe-Cr interaction parameters used to successfully predict growth kinetics in the Fe-C-1Mn (at 730°C) and Fe-C-1Cr (at 750°C) alloys were used to model the expected kinetics in the quaternary Fe-C-Mn-Cr system. It must be noted that ferrite growth kinetics could not be modeled in the Fe-C-Cr system at 730°C due to pearlite formation. Like in the ternary systems, the Fe-C interaction parameter (${}^0L_{Fe:C,Va}$) at the interface was adjusted to -50 $kJ.mol^{-1}$, and the Mn-C and Cr-C Wagner interaction parameters (ϵ_{MnC} and ϵ_{CrC}) were modified to capture the same Wagner interaction parameters as in austenite for both Mn and Cr. As mentioned before, the modification of the Fe-Mn (${}^0L_{Fe,Mn:Va}$) and Fe-Cr (${}^0L_{Fe,Cr:Va}$) parameters induces a modification of the Mn-Cr Wagner interaction parameter (ϵ_{MnCr}). In the present study, this parameter

was adjusted to capture the same Mn-Cr Wagner interaction as in austenite. Good agreement was obtained between the model predictions and the experimental results as shown in figure 10. This agreement is especially significant since the parameters used to successfully predict the growth kinetics were directly extracted from the ternary systems and no further calibration was needed.

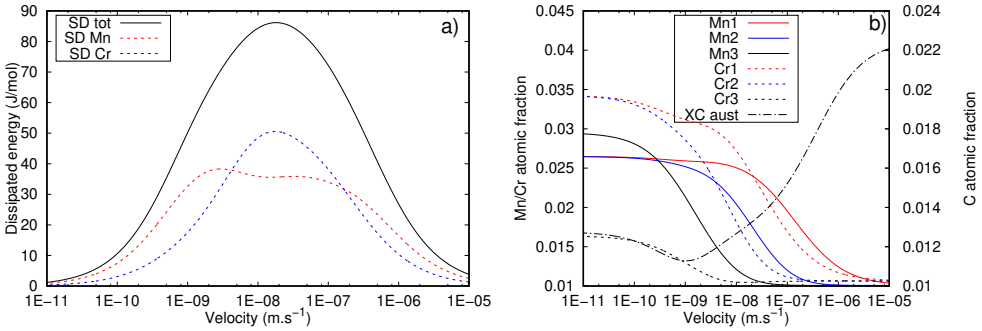

Figure 15: a) The dissipated free energy due Mn and Cr elements diffusion across the interface as function of the interface velocity for Fe-0.26C-1Mn-1Cr at 730°C. b) The evolution of Mn and Cr contents at the different atomic planes of the interface as well as the carbon content at the austenite interface side as function of interface velocity.

The dissipated energies due to manganese and chromium diffusion across the interface as function of the interface velocity are shown in figure 15-a. The maximal total dissipated energy (86 $J.mol^{-1}$) is reached at medium velocities ($5e^{-8}$ $m.s^{-1}$). The maximal dissipated energy of Mn and Cr are 38 $J.mol^{-1}$ and 50 $J.mol^{-1}$, respectively. When comparing with the obtained dissipated energies for the ternary systems (Fe-0.26C-1Mn and Fe-0.26C-1Cr) at the same temperature using the same binding energies, the maximal dissipated energies for Mn and Cr were 44 $J.mol^{-1}$ and 96 $J.mol^{-1}$, respectively.

Figure 15-b shows the evolution of Mn and Cr contents at the different interface atomic planes as well as the evolution of C at the austenite side of the interface as function of velocity. Both Mn and Cr show the same segregation behavior as in the ternary systems. The Mn and Cr contents start to deviate from PE conditions and segregate at the different atomic layers with decreasing velocity. A higher maximum segregation of Cr is reached at low velocities compared to Mn (Cr : $K_{max} = 3.18$, Mn : $K_{max} = 2.64$).

The manganese enrichment factor in the Fe-C-Mn-Cr alloy is similar to that calculated in the ternary Fe-C-Mn system (2.9). On the other hand, the chromium enrichment factor obtained for the quaternary Fe-C-Mn-Cr system is lower than that calculated in the ternary Fe-C-Cr system at the same temperature, 730°C (K_{max} : 5). It has to be noted that the interaction between chromium and manganese is slightly attractive (ϵ_{CrMn} : -0.13) and thus cannot be the origin of the observed segregation behavior. The calculated effective binding energies for manganese and chromium are, -3.8 $kJ.mol^{-1}$ and -9.2 $kJ.mol^{-1}$ respectively.

To highlight the effect of taking in consideration the different interaction parameters (Fe-C, Mn-C, Cr-C and Mn-Cr), the solute drag model was applied to the Fe-C-1Mn-1Cr system under three different sets of hypothesis:

a) the Fe-C (${}^0L_{Fe:C,Va}$) interaction parameter is not modified, the Mn-C (ϵ_{MnC}), Cr-C (ϵ_{CrC}) and Mn-Cr (ϵ_{MnCr}) Wagner interaction parameters are not adjusted.

b) only the Fe-C (${}^0L_{Fe:C,Va}$) interaction parameter was modified

a) the Fe-C interaction parameter (${}^0L_{Fe:C,Va}$) is modified, the Mn-C and Cr-C Wagner interaction parameters (ϵ_{MnC} and ϵ_{CrC}) are adjusted to their values in autenite, the Mn-Cr Wagner interaction parameter (ϵ_{MnCr}) is not adjusted to its value in austenite.

In all cases, the same Fe-Mn and Fe-Cr interaction parameters used to obtain the best fit in ternary systems Fe-C-Mn and Fe-C-Cr were used in to model the quaternary Fe-C-Mn-Cr.

The calculated kinetics and the measured one are plotted in figure 16.

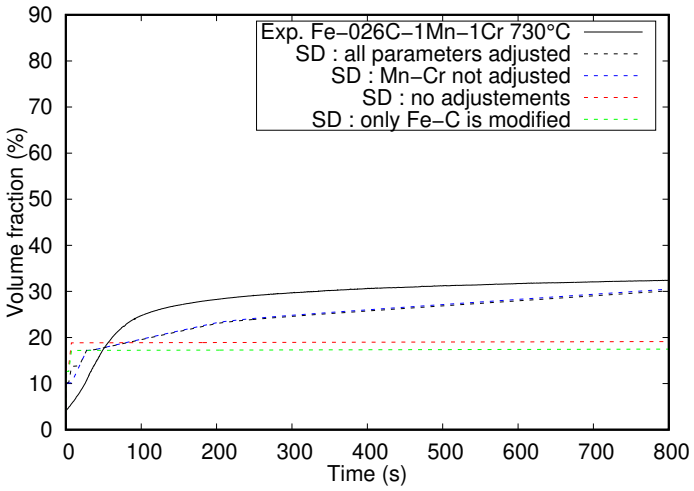

Figure 16: Comparison between the measured ferrite growth kinetics (solid black line) of the Fe-0.26C-1Mn-1Cr at 730°C, and the predictions of the solute drag (dashed lines) model obtained using different approaches in the description of the interaction parameters.

In a first stage, no modifications were made on the Fe-C, Mn-C, Cr-C and Mn-Cr interaction parameters. The model predicts a faster growth kinetic and a lower final fraction compared to measurements. As already mentioned, the used Fe-Mn and Fe-Cr interaction parameters gave good results for the ternary systems. A similar result was obtained when only the Fe-C interaction parameter (${}^0L_{Fe:C,Va}$) was modified (-50 $kJ.mol^{-1}$) and no adjustments were conducted on the Mn-C, Cr-C and Mn-Cr Wagner interaction parameters.

When the Fe-C (${}^0L_{Fe:C,Va}$), Mn-C (ϵ_{MnC}) and Cr-C (ϵ_{CrC}) parameters are modified and the Mn-Cr (ϵ_{MnCr}) is not adjusted, the obtained kinetics are in good agreement with the experimental result. The dissipated energy and the segregated values are similar to the case where the all the interaction parameters were modified. This can be explained by the small difference in the Mn-Cr Wagner interaction parameter (ϵ_{MnCr}) between austenite and the interface caused by the modification of the Fe-Mn (${}^0L_{Fe,Mn:Va}$) and Fe-Cr (${}^0L_{Fe,Cr:Va}$) fitting interaction parameters.

These results highlight the importance of considering the whole thermodynamic description of the different interaction parameters when modeling ferrite growth kinetics in multicomponent

systems. The interactions of all the elements in the system should be accounted for, especially those of substitutional elements with carbon, which have significant effects on the segregation behaviors of those elements, and as a result, on ferrite growth kinetics as well.

6. Conclusion

The effect of alloying elements and temperature on ferrite growth kinetics during austenite to ferrite phase transformation was studied using HEXRD experiments in different ternary Fe-C-X systems (where X : Mn, Ni, Mo and Cr) as well as in a quaternary Fe-C-Cr-Mn system. The comparison between the experimental results and the classical PE and LE models showed that these models cannot be used to describe ferrite growth kinetics in all conditions. Moreover, the Fe-C-Mo and Fe-C-Cr systems showed ferrite growth kinetics slower than both LE and PE predictions, indicating that the transformation generally proceeds under conditions differing from the hypotheses of those models. These experimental results were compared to the predictions of a modified version of the solute drag model initially developed by Zurob et al. [12]. In the present version of the model, the interaction between carbon and iron at the interface was modified to account for the significant carbon segregation at the austenite ferrite interface reported in the literature. Moreover, it was shown that the calibration of inter-elemental interactions must be carried out in a comprehensive manner as their effect on the calculated transformation rate can be significant. In particular, it was shown that interactions with carbon can severely affect the segregation behavior of substitutional elements, and in turn, the drag they exert on the interface. The comparison between the measured kinetics and the solute drag model predictions showed good agreement for almost all studied systems. It has to be mentionned again that only one fitting paramter (i.e the Fe-X interactin parameter expressed using the $L_{Fe,X:Va}$ parameter) was used in the present version of the solute drag model.Table 7 summarizes the $L_{Fe,Xn:Va}$ parameters used to get the best fit of the experimental kinetics as well as their corresponding binding energies (E_0), calculated at the para-equilibrium conditions. The estimated intrinsic segregation energies showed a weak affinity of manganese for the interface and that its segregation is enhanced by the presence of carbon at the interface. Nickel on the other hand is predicted to segregate highly to the interface, in contrast to reported observations at grain boundaries and interfaces. The tendency of molybdenum and chromium to segregate at the interface is also enhanced by the presence of carbon at the interface. The solute drag model was also applied successfully to the quaternary Fe-C-Mn-Cr system using the parameters of the ternary sub-systems.

These results illustrate the importance of an exhaustive calibration of the inter-elemental interactions at the interface and show that solute drag models could lead to reliable and universal modeling of the transformation of austenite into ferrite in multi-component steel grades.

Table 7: The Fe-X interaction parameters (${}^0L_{Fe,X:Va}$) as well as the corresponding binding energies E_0 used in the solute drag modeling for the Fe-C-X systems.

T(°C)	Fe-C-X	${}^0L_{Fe,X:Va}$ $(kJ.mol^{-1})$	E_0 $(kJ.mol^{-1})$
730	0.3Mn	-1.4	+1.5
750	0.3Mn	-1.6	+1.5
775	0.3M	-1.9	+1.5
730	0.7Mn	-1.5	+1.5
750	0.7Mn	-1.7	+1.5
775	0.7Mn	-2.0	+1.5
730	1Mn	-1.7	+1.5
750	1Mn	-1.8	+1.5
775	1Mn	-2.1	+1.5
730	1Ni	-11.7	-6.5
750	1Ni	-11.8	-6.5
775	1Ni	-11.9	-6.5
730	0.2Mo	-7.2	-15
750	0.2Mo	-7.5	-15
775	0.2Mo	-7.9	-15
750	1Cr	+5.1	+1.5
775	1Cr	-4.9	-1.5

Acknowledgements

We acknowledge DESY (Hamburg, Germany), a member of the Helmholtz Association HGF, for the provision of experimental facilities. Parts of this research were carried out at PETRA III and we would like to thank Dr. U. Lienert and Dr. Z. Hegedues for assistance in using beamline P21.2. Prof. H.S. Zurob is acknowledged for stimulating discussion and valuable input regarding solute drag modelling. Dr. Florence Robaut is acknowledged for her support with the EPMA measurements. This work was supported by the ANR (Agence Nationale de la Recherche [ANR-15-IDEX-02] and by MIAI@Grenoble Alpes [ANR-19-P3IA-0003].

References

[1] H. Bhadeshia, R. Honeycombe, Steels: Microstructure and Properties, Elsevier, 2011, google-Books-ID: 6MtuBqok43MC.

[2] H. K. D. H. Bhadeshia, Diffusional formation of ferrite in iron and its alloys, Progress in Materials Science 29 (4) (1985) 321–386. doi:10.1016/0079-6425(85)90004-0.
URL http://www.sciencedirect.com/science/article/pii/0079642585900040

[3] M. Enomoto, Comparison of alloy element partition behavior and growth kinetics of proeutectoid ferrite in Fe-C-X alloys with diffusion growth theory., ISIJ Int. 28 (10) (1988) 826–835. doi:10.2355/isijinternational1966.28.826.
URL http://joi.jlc.jst.go.jp/JST.Journalarchive/isijinternational1966/28.826?from=CrossRef

[4] M. ENOMOTO, Local Conditions at Moving a/g Boundaries of Proeutectoid Ferrite Transformation in Iron Alloys, METALLURGICAL AND MATERIALS TRANSACTIONS A 8.

[5] J. B. Gilmour, G. R. Purdy, J. S. Kirkaldy, Partition of manganese during the proeutectoid ferrite transformation in steel, Metallurgical Transactions 3 (12) (1972) 3213–3222. doi:10.1007/BF02661336.
URL http://link.springer.com/10.1007/BF02661336

[6] K. Oi, C. Lux, G. Purdy, A study of the influence of Mn and Ni on the kinetics of the proeutectoid ferrite reaction in steels, Acta Materialia 48 (9) (2000) 2147–2155. doi:10.1016/S1359-6454(00)00041-0.
URL https://linkinghub.elsevier.com/retrieve/pii/S1359645400000410

[7] A. Van der Ven, L. Delaey, Models for precipitate growth during the $\gamma \rightarrow \alpha + \gamma$ transformation in Fe-C and Fe-C-M alloys, Progress in Materials Science 40 (3) (1996) 181–264. doi:10.1016/0079-6425(96)00002-3.
URL http://www.sciencedirect.com/science/article/pii/0079642596000023

[8] M. Hillert, Nature of local equilibrium at the interface in the growth of ferrite from alloyed austenite, Scripta materialia 46 (6) (2002) 447–453.

[9] D. E. Coates, Diffusion-controlled precipitate growth in ternary systems I, Metallurgical and Materials Transactions B 3 (5) (1972) 1203–1212.

[10] M. Gouné, F. Danoix, J. Ågren, Y. Bréchet, C. Hutchinson, M. Militzer, G. Purdy, S. van der Zwaag, H. Zurob, Overview of the current issues in austenite to ferrite transformation and the role of migrating interfaces therein for low alloyed steels, Materials Science and Engineering: R: Reports 92 (2015) 1–38. doi:10.1016/j.mser.2015.03.001.
URL http://linkinghub.elsevier.com/retrieve/pii/S0927796X15000248

[11] C. R. Hutchinson, A. Fuchsmann, Y. Brechet, The diffusional formation of ferrite from austenite in Fe-C-Ni alloys, Metallurgical and Materials Transactions A 35 (4) (2004) 1211–1221. doi:10.1007/s11661-004-0295-1.
URL http://link.springer.com/10.1007/s11661-004-0295-1

[12] H. S. Zurob, D. Panahi, C. R. Hutchinson, Y. Brechet, G. R. Purdy, Self-Consistent Model for Planar Ferrite Growth in Fe-C-X Alloys, Metallurgical and Materials Transactions A 44 (8) (2013) 3456–3471. doi:10.1007/s11661-012-1479-8.
URL http://link.springer.com/10.1007/s11661-012-1479-8

[13] M. Hillert, B. Sundman, A treatment of the solute drag on moving grain boundaries and phase interfaces in binary alloys, Acta Metallurgica 24 (8) (1976) 731–743. doi:10.1016/0001-6160(76)90108-5.
URL http://linkinghub.elsevier.com/retrieve/pii/0001616076901085

[14] C. Qiu, The 'Solute-Drag' Effect on Migrating Interfaces during Solid-State Phase Transformations, Ph.D. thesis.

[15] C. Qiu, H. Zurob, C. Hutchinson, The coupled solute drag effect during ferrite growth in Fe–C–Mn–Si alloys using controlled decarburization, Acta Materialia 100 (2015) 333–343. doi:10.1016/j.actamat.2015.08.065.
URL http://linkinghub.elsevier.com/retrieve/pii/S1359645415006527

[16] W. Sun, H. Zurob, C. Hutchinson, Coupled solute drag and transformation stasis during ferrite formation in Fe-C-Mn-Mo, Acta Materialia 139 (2017) 62–74. doi:10.1016/j.actamat.2017.08.010.
URL https://linkinghub.elsevier.com/retrieve/pii/S1359645417306535

[17] T. Tanaka, H. I. Aaronson, M. Enomoto, Growth Kinetics of Grain Boundary AIIotriomorphs of Proeutectoid Ferrite in Fe-C-Mn-X2 Alloys, METALLURGICAL AND MATERIALS TRANSACTIONS A 20.

[18] H. Guo, G. R. Purdy, M. Enomoto, H. I. Aaronson, Kinetic transitions and substititional solute (Mn) fields associated with later stages of ferrite growth in Fe-C-Mn-Si, Metallurgical and Materials Transactions A 37 (6) (2006) 1721–1729. doi:10.1007/s11661-006-0115-x.
URL http://link.springer.com/10.1007/s11661-006-0115-x

[19] H. I. Aaronson, W. T. Reynolds, G. R. Purdy, Coupled-solute drag effects on ferrite formation in Fe-C-X systems, Metallurgical and Materials Transactions A 35 (4) (2004) 1187–1210. doi:10.1007/s11661-004-0294-2.
URL http://link.springer.com/10.1007/s11661-004-0294-2

[20] M. Enomoto, C. White, H. Aaronson, Evaluation of the effects of segregation on austenite grain boundary energy in fe-cx alloys, Metallurgical Transactions A 19 (7) (1988) 1807–1818.

[21] M. Enomoto, Influence of solute drag on the growth of proeutectoid ferrite in Fe–C–Mn alloy, Acta materialia 47 (13) (1999) 3533–3540.

[22] H. Guo, M. Enomoto, Effects of Substitutional Solute Accumulation at α/γ Boundaries on the Growth of Ferrite in Low Carbon Steels, Metallurgical and Materials Transactions A 38 (6) (2007)

1152–1161. doi:10.1007/s11661-007-9139-0.
URL http://link.springer.com/10.1007/s11661-007-9139-0
[23] S. H. Lee, K. S. Lee, K. J. Lee, Evaluation of Wagner Interaction Parameter in Fe-Mn-Si-Nb-Ti-V-C System, MSF 475-479 (2005) 3327–3330. doi:10.4028/www.scientific.net/MSF.475-479.3327.
URL https://www.scientific.net/MSF.475-479.3327
[24] H. P. Van Landeghem, B. Langelier, D. Panahi, G. R. Purdy, C. R. Hutchinson, G. A. Botton, H. S. Zurob, Solute Segregation During Ferrite Growth: Solute/Interphase and Substitutional/Interstitial Interactions, JOM 68 (5) (2016) 1329–1334. doi:10.1007/s11837-016-1852-y.
URL http://link.springer.com/10.1007/s11837-016-1852-y
[25] F. Danoix, X. Sauvage, D. Huin, L. Germain, M. Gouné, A direct evidence of solute interactions with a moving ferrite/austenite interface in a model Fe-C-Mn alloy, Scripta Materialia 121 (2016) 61–65. doi:10.1016/j.scriptamat.2016.04.038.
URL http://www.sciencedirect.com/science/article/pii/S135964621630166X
[26] A. Béché, H. Zurob, C. Hutchinson, Quantifying the Solute Drag Effect of Cr on Ferrite Growth Using Controlled Decarburization Experiments, Metallurgical and Materials Transactions A 38 (12) (2007) 2950–2955. doi:10.1007/s11661-007-9353-9.
URL http://link.springer.com/10.1007/s11661-007-9353-9
[27] C. R. Hutchinson, H. S. Zurob, Y. Bréchet, The growth of ferrite in Fe-C-X alloys: The role of thermodynamics, diffusion, and interfacial conditions, Metallurgical and Materials Transactions A 37 (6) (2006) 1711–1720. doi:10.1007/s11661-006-0114-y.
URL http://link.springer.com/10.1007/s11661-006-0114-y
[28] A. Phillion, H. W. Zurob, C. R. Hutchinson, H. Guo, D. V. Malakhov, J. Nakano, G. R. Purdy, Studies of the influence of alloying elements on the growth of ferrite from austenite under decarburization conditions: Fe-C-Nl alloys, Metallurgical and Materials Transactions A 35 (4) (2004) 1237–1242. doi:10.1007/s11661-004-0297-z.
URL http://link.springer.com/10.1007/s11661-004-0297-z
[29] H. Chen, B. Appolaire, S. van der Zwaag, Application of cyclic partial phase transformations for identifying kinetic transitions during solid-state phase transformations: Experiments and modeling, Acta Materialia 59 (17) (2011) 6751–6760. doi:10.1016/j.actamat.2011.07.033.
URL https://linkinghub.elsevier.com/retrieve/pii/S135964541100509X
[30] X. Sun, H. Dong, Q. Liu, Y. Weng, Dynamically transformed ferrite fraction inferred from dilatometry measurements after deformation, Materials Science and Engineering: A 487 (1-2) (2008) 93–98. doi:10.1016/j.msea.2007.09.065.
URL https://linkinghub.elsevier.com/retrieve/pii/S0921509307017042
[31] L. Zhao, T. A. Kop, V. Rolin, J. Sietsma, A. Mertens, P. J. Jacques, Quantitative dilatometric analysis of intercritical annealing in a low-silicon TRIP steel 7.
[32] V. Esin, B. Denand, Q. Le Bihan, M. Dehmas, J. Teixeira, G. Geandier, S. Denis, T. Sourmail, E. Aeby-Gautier, In situ synchrotron X-ray diffraction and dilatometric study of austenite formation in a multi-component steel: Influence of initial microstructure and heating rate, Acta Materialia 80 (2014) 118–131. doi:10.1016/j.actamat.2014.07.042.
URL https://linkinghub.elsevier.com/retrieve/pii/S1359645414005606
[33] G. Geandier, E. Aeby-Gautier, A. Settefrati, M. Dehmas, B. Appolaire, Study of diffusive transformations by high energy X-ray diffraction, Comptes Rendus Physique 13 (3) (2012) 257–267. doi:10.1016/j.crhy.2011.12.001.
URL https://linkinghub.elsevier.com/retrieve/pii/S1631070511002635
[34] S. Catteau, H. Van Landeghem, J. Teixeira, J. Dulcy, M. Dehmas, S. Denis, A. Redjaïmia, M. Courteaux, Carbon and nitrogen effects on microstructure and kinetics associated with bainitic transformation in a low-alloyed steel, Journal of Alloys and Compounds 658 (2016) 832–838. doi:10.1016/j.jallcom.2015.11.007.
URL https://linkinghub.elsevier.com/retrieve/pii/S0925838815315632
[35] A. Bénéteau, P. Weisbecker, G. Geandier, E. Aeby-Gautier, B. Appolaire, Austenitization and precipitate dissolution in high nitrogen steels: an in situ high temperature X-ray synchrotron diffraction analysis using the Rietveld method, Materials Science and Engineering: A 393 (1-2) (2005) 63–70. doi:10.1016/j.msea.2004.09.054.
URL https://linkinghub.elsevier.com/retrieve/pii/S0921509304011797
[36] B. Denand, M. Dehmas, E. Gautier, C. Bonnet, G. Geandier, J.-P. Sarteaux, PORTABLE ANALYSIS OVEN FOR RADIATION LINE (Apr. 2019).
URL https://patents.google.com/patent/FR3072777A1/fr?q=PORTABLE+ANALYSIS+OVEN+FOR+RADIATION+LINEoq=PORTABLE+ANA
[37] J. Kieffer, D. Karkoulis, Pyfai, a versatile library for azimuthal regrouping, in: J. Phys. Conf. Ser,

Vol. 425, 2013, p. 36.
[38] J. Rodriguez-Carvajal, Fullprof: a program for rietveld refinement and pattern matching analysis, in: satellite meeting on powder diffraction of the XV congress of the IUCr, Vol. 127, Toulouse, 1990.
[39] H. Dong, Y. Zhang, G. Miyamoto, H. Chen, Z. Yang, T. Furuhara, A comparative study on intrinsic mobility of incoherent and semicoherent interfaces during the austenite to ferrite transformation, Scripta Materialia 188 (2020) 59–63. doi:10.1016/j.scriptamat.2020.07.007.
URL https://linkinghub.elsevier.com/retrieve/pii/S1359646220304462
[40] F. Fazeli, M. Militzer, Application of solute drag theory to model ferrite formation in multiphase steels, Metallurgical and Materials Transactions A 36 (6) (2005) 1395–1405. doi:10.1007/s11661-005-0232-y.
URL http://link.springer.com/10.1007/s11661-005-0232-y
[41] H. Farahani, W. Xu, S. van der Zwaag, Prediction and Validation of the Austenite Phase Fraction upon Intercritical Annealing of Medium Mn Steels, Metall and Mat Trans A 46 (11) (2015) 4978–4985. doi:10.1007/s11661-015-3081-3.
URL http://link.springer.com/10.1007/s11661-015-3081-3
[42] H. I. Aaronson, Lectures on the theory of phase transformations, Metallurgical Society of AIME, 1975.
[43] H. Van Landeghem, B. Langelier, B. Gault, D. Panahi, A. Korinek, G. Purdy, H. Zurob, Investigation of solute/interphase interaction during ferrite growth, Acta Materialia 124 (2017) 536–543. doi:10.1016/j.actamat.2016.11.035.
URL http://linkinghub.elsevier.com/retrieve/pii/S1359645416309028
[44] C. Qiu, H. S. Zurob, D. Panahi, Y. J. M. Brechet, G. R. Purdy, C. R. Hutchinson, Quantifying the Solute Drag Effect on Ferrite Growth in Fe-C-X Alloys Using Controlled Decarburization Experiments, Metallurgical and Materials Transactions A 44 (8) (2013) 3472–3483. doi:10.1007/s11661-012-1547-0.
URL http://link.springer.com/10.1007/s11661-012-1547-0
[45] H. Chen, S. van der Zwaag, A general mixed-mode model for the austenite-to-ferrite transformation kinetics in Fe–C–M alloys, Acta Materialia 72 (2014) 1–12. doi:10.1016/j.actamat.2014.03.034.
URL http://linkinghub.elsevier.com/retrieve/pii/S1359645414001815
[46] H. Zurob, C. Hutchinson, Y. Bréchet, H. Seyedrezai, G. Purdy, Kinetic transitions during non-partitioned ferrite growth in Fe–C–X alloys, Acta Materialia 57 (9) (2009) 2781–2792. doi:10.1016/j.actamat.2009.02.029.
URL https://linkinghub.elsevier.com/retrieve/pii/S135964540900127X
[47] D. Panahi, Y. F. Bai, H. S. Zurob, G. R. Purdy, C. R. Hutchinson, Y. Bréchet, Kinetic Transitions during Non-Partitioned Ferrite Growth in Fe-C-Mn Alloys, Solid State Phenomena 172-174 (2011) 539–548. doi:10.4028/www.scientific.net/SSP.172-174.539.
URL http://www.scientific.net/SSP.172-174.539
[48] W. CAHNt, EFFECT IN GRAIN BOUNDARY MOTION 10.
[49] D. Panahi, Effect of alloying elemnts on ferrite growth in fe-c-x ternary alloys, Ph.D. thesis (2013).
[50] M. Guttmann, Equilibrium segregation in a ternary solution: A model for temper embrittlement, Surface Science 53 (1) (1975) 213–227.
[51] B. Uhrenius, A compendium of ternary iron-base phase diagrams, Proc. of a Sympo. on Hardenability Concepts with Applications to Steel 28 (1977).
[52] N. Maruyama, G. Smith, A. Cerezo, Interaction of the solute niobium or molybdenum with grain boundaries in α-iron, Materials Science and Engineering: A 353 (1-2) (2003) 126–132.
[53] B. Sundman, J. Ågren, A regular solution model for phases with several components and sublattices, suitable for computer applications, Journal of Physics and Chemistry of Solids 42 (4) (1981) 297–301. doi:10.1016/0022-3697(81)90144-X.
URL https://linkinghub.elsevier.com/retrieve/pii/002236978190144X

Supplementary material

Solute drag modeling

We developed a modified version of the three-jump solute drag model proposed by Zurob et al. [12] to predict the effect of composition and temperature on ferrite growth kinetics. Zurob et al.[12] used Hillert's [13] approach tto develop a discrete model of mass transport across the interface to evaluate solute drag during ferrite growth in Fe-C-X systems. In this model, the austenite-ferrite interface is considered as a two atomic layer thick discrete interface. During ferrite growth, diffusion of substitutional elements across the interface involves three jumps across the interface, from ferrite to the first atomic layer, a second jump within the interface and a final jump to austenite. As a result, an atomic flux of solute atoms is generated due to the difference of thermodynamic properties across the interface. The composition of alloying elements in each of these atomic planes is estimated using a mass balance equation:

$$dx_X^i \frac{\delta}{V_m dt} = J_X^i - J_X^{i+1} + \frac{v}{V_m}(x_X^{i+1} - x_X^i) \tag{S1}$$

where v is the interface velocity and J^i is the flux of the solute element from plane $i-1$ to plane i and is expressed as follows :

$$J_X^i = -\frac{D_X^i}{V_m RT} x_{Fe}^{i-1} x_X^{i-1} \frac{(\mu_X^i - \mu_X^{i-1}) - (\mu_{Fe}^i - \mu_{Fe}^{i-1})}{\delta} \tag{S2}$$

where μ_X^i and μ_{Fe}^i are the respective chemical potentials of X and Fe at plane i, δ is the interface thickness, V_m is the molar volume, R is the gas constant, T is temperature and D_i is the diffusion coefficient of element X from plane $i-1$ to plane i. Assuming a steady state, the composition of X in each plane can be evaluated from Eq.S1 and S2. The dissipated energy due to diffusion is then estimated using Hillert's approach [13]:

$$\Delta G_m^{diss,X} = \sum_{i=1}^{i=3} -\frac{V_m}{v} J_X^i [(\mu_X^i - \mu_X^{i-1}) - (\mu_{Fe}^i - \mu_{Fe}^{i-1})] \tag{S3}$$

and the total dissipated energy due to diffusion of all substitutional elements is given by :

$$\Delta G_m^{diss} = \sum^{X} \Delta G_m^{diss,X} \tag{S4}$$

The local energy balance at the interface is used to calculate the interfacial conditions during ferrite growth.

$$\Delta G_m^{chem} = \Delta G_m^{diss} + \Delta G_m^{fric} = 0 \tag{S5}$$

The interface mobility is considered large enough for the dissipated energy due to interface friction to be neglected in the present model [14, 11]. Moreover, interface friction mainly contributes at very high ($> 10e^{-6}$ $m.s^{-1}$) and very low velocities ($< 10e^{-11}$ $m.s^{-1}$), which are not the operating velocities during precipitation or decarburization experiments [14]. The driving force is expressed in terms of substitutional elements as follows:

$$\Delta G_m^{chem} = \sum^{X} \left\{ \frac{(u_X^{\alpha} + u_X^{\gamma})}{2} (\mu_X^{\gamma,i} - \mu_X^{\alpha,i}) \right\} + \frac{(u_{Fe}^{\alpha} + u_{Fe}^{\gamma})}{2} (\mu_{Fe}^{\gamma,i} - \mu_{Fe}^{\alpha,i}) \tag{S6}$$

Where $u_{Fe} = \frac{X_{Fe}}{1-X_C}$ and $u_X == \frac{X_X}{1-X_C}$ are the molar fraction of X and Fe elements at the austenite and ferrite interface sides. The interface is considered to be initially in PE mode and the interface velocity is evaluated from carbon diffusion in bulk phases (ferrite and austenite in decarburization and austenite only in precipitation):

$$v = \frac{J_C^{\gamma} - J_C^{\alpha}}{x_C^{i,\gamma} - x_C^{i,\alpha}} \tag{S7}$$

The carbon chemical potential is assumed constant across the interface. The thermodynamic properties of the interface are described using an approach developed by Hillert [12, 42]. The interface properties are modified from those of austenite by shifting the reference state for the free energy by $3.5 kJ.mol^{-1}$. This value was chosen to capture an interfacial energy of 0.5 J.m^{-2}. TCFE9 and MOB2 databases of ThermoCalc and DICTRA were used to calculate the different thermodynamic properties in austenite and ferrite such as chemical potentials and diffusion coefficients. In the present study, and in order to capture the significant segregation of carbon at the interface observed using atom probe experiments [25, 43], the 'L' interaction parameter between carbon and iron at the interface was adjusted from -34 $kJ.mol^{-1}$ (as in austenite) to -50 $kJ.mol^{-1}$ (as shown in Fig.S6 and Fig.S7). This parameter is explained further in the text. A key feature of Zurob's model is the choice of two parameters: the binding energy of the substitutional element at the interface and the trans-interface diffusion coefficient of the solute element. These two parameters are not known experimentally and generally used as fitting parameters. The binding energy is generally defined as the difference between the chemical potential of X at the interface and the average chemical potentials of X in ferrite and austenite as shown in figure S1 [12, 44, 45]. ΔE is the average of the solute chemical potential difference between austenite and ferrite, μ_X^{α} and μ_X^{γ} are the chemical potential of the substitutional solute in ferrite and austenite, respectively. The binding energy is here modified throught the ${}^0L_{Fe,X:Va}$ interaction parameter as follows :

The binding energy E_0 is calculated using :

$$E_0 = \frac{(\mu_X^{\gamma} + \mu_X^{\alpha})}{2} - \mu_X^{boun} \tag{S8}$$

The chemical potential of element X at the interface is modified to obtain the desired binding energy, using :

$$\mu_X = \mu_X^0 + RT \ln(Y_X) + RT \frac{c}{a} \ln(1 - Y_C) + {}^E G_X \tag{S9}$$

where :

$$\begin{aligned} {}^a G_X = Y_{Fe} Y_C (\Delta G + L(Fe, X:Va) - L(Fe, X:C) + L(X:C, Va) \\ - L(Fe:C, Va)) + Y_{Fe}^2 L(Fe, X:Va) + Y_C^2 L(X:C, Va) \\ + Y_{Fe}^2 Y_C 2(L(Fe, X:C) - L(Fe, X:Va)) \\ + Y_{Fe} Y_C^2 2(L(Fe:C, Va) - L(X:C, Va)) \end{aligned} \tag{S10}$$

Y_i is site fraction. a and c are the number of sites per mole. For austenite a=1, c=1. For ferrite a=1, c=3 and

$$L(i:j) = \sum^{k} {}^{k}L(Y_i - Y_j)^k \tag{S11}$$

The choice of the ${}^{0}L_{Fe,X:Va}$ interaction parameter to express the segregation behaviour of element X at the interface was initially proposed by Zurob et al. [12], based on the initial proposition by Hillert [42]. One should note that other parameters, including for instance ${}^{0}L_{X:Va}$, can also be used to express this segregation. However, the choice made here enabled consistency with the original three-jump model [12].

The binding energy parameter has been used to express the segregation behavior of the substitutional element at the interface [12, 14, 15, 45, 46, 47]. However, this parameter as calculated with this approach depends on the conditions under which the calculations are made. Carbon segregation and thus interface velocity highly impacts the calculated binding energy.

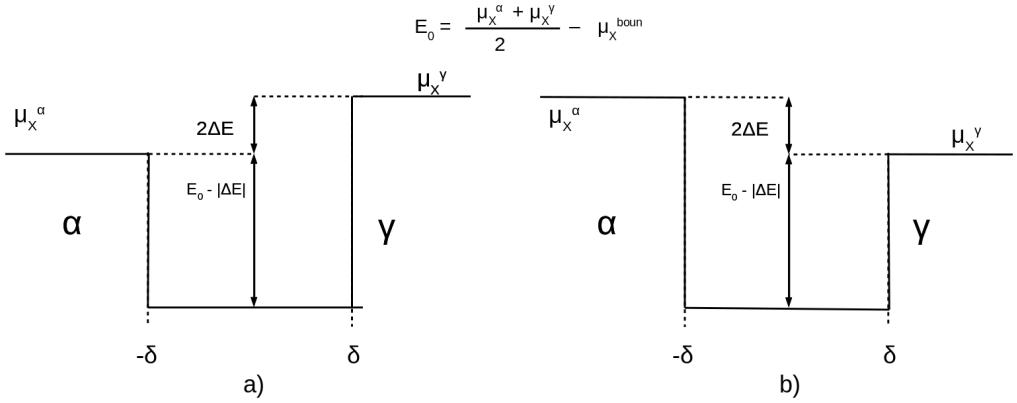

Figure S1: Schematic illustration of the potential well for (a) ferrite stabilizer and (b) austenite stabilizer inside the interface and the calculation of the binding energy in solute drag models.

In the present study, the segregation behavior was discussed in terms of enrichment factor calculated at slow velocities (when equilibrium conditions are approached).

In the present study, diffusion coefficients for the different jumps were chosen as: the diffusion coefficient of element X in ferrite D_α for D_1 , the diffusion coefficient in austenite D_γ as D_3 and the geometrical average of D_α and D_γ as D_2. It is important to note that this assumption was used for all the studied systems. As a result, interface diffusion is not a fitting parameter as in previous studies [44]. The only fitting parameter used in the present study is the interaction parameter between Fe and X element at the interface. It has to be noted that this parameter does not express directly the segregation behavior of element X at the interface. The segregation behavior of element X at the interface depends on a set of interaction parameters, namely those for Fe-X, Fe-C, X-C and X_1-X_2 (in case of two substitutional solutes). For example, an element with a high affinity to carbon such as molybdenum will highly segregate at the interface due

to the presence of carbon [27]. The interaction between Fe and X element is expressed using the ${}^{0}\mathrm{L}_{Fe,X:Va}$ thermodynamic parameter in the ThermoCalc database and the Fe-C interaction parameter is expressed using ${}^{0}\mathrm{L}_{Fe:C,Va}$ parameter. The interaction parameter between X and C at the interface is estimated using the Wagner interaction parameter as function of the different L parameters as shown by Eq.S12 [23]

$$\begin{aligned}\epsilon_{XC} = -\{\ ({}^{0}L_{Fe,X:Va} + {}^{1}L_{Fe,X:Va} + {}^{2}L_{Fe,X:Va}) + ({}^{0}L_{Fe:C,Va} - {}^{1}L_{Fe:C,Va} + \\ {}^{2}L_{Fe:C,Va}) - ({}^{0}L_{X:C,Va} - {}^{1}L_{X:C,Va} + {}^{2}L_{X:C,Va}) - ({}^{0}L_{Fe,X:C} + {}^{1}L_{Fe,X:C} \\ + {}^{2}L_{Fe,X:C}) - L_{Fe,X:C,Va}\ \}/RT\end{aligned} \tag{S12}$$

where ϵ_{XC} is the Wagner interaction parameter between X and C elements, expressed in the two-sublattice model [53], where one sublattice is occupied by the substitutional solute elements and the second one by the interstitial elements (carbon). The thermodynamic parameters L describe the mutual interaction between two elements. $\mathrm{L}_{Fe,X:Va}$ and $\mathrm{L}_{Fe,X:C}$ express the interaction between Fe and X elements when the first sub-lattice is occupied by Fe and X elements and the second sub-lattice by interstitial vacancies V_a and carbon, respectively. The left side superscripts on the L parameters express the coefficients of the Redlich-Kister polynomial order.

As it is shown by Eq.S12, the Wagner interaction parameter ϵ_{XC} is affected by the Fe-X and Fe-C interaction parameters (${}^{0}L_{Fe,X:Va}$ and ${}^{0}L_{Fe:C,Va}$, respectively). Consequently, changing these two parameters, Fe-X (to fit the experimental results) and Fe-C (to express the high carbon segregation at the interface) results in a modification of the interaction behavior between carbon and the solute element at the interface. In the present study, the interaction between X and C at the interface was considered to have the same value as in austenite [20]. To this end, the Wagner interaction parameter (ϵ_{XC}) is calculated both in austenite and at the interface using Eq.S12 and the difference is adjusted by modifying the $L_{Fe,X:C,Va}$ parameter of the interface.

In quaternary systems, the Wagner interaction between the two solutes X_1 and X_2 ($\epsilon_{X_1X_2}$) at the interface is expressed using Eq.S13. This parameter is impacted by the Fe-X1 and Fe-X2 interaction parameters. Again, the X_1-X_2 interaction parameter in the interface is assumed similar to the one in austenite [20]. Once the Fe-X_1 and Fe-X_2 interaction parameters are adjusted, the Wagner interaction parameter between X_1 and X_2 is calculated in both austenite and the interface and the $L_{X1,X2:Va}$ parameter of the interface is adjusted to capture the same X_1-X_2 Wagner parameter as in austenite.

$$\begin{aligned}\epsilon_{X1X2} = -\{\ ({}^{0}L_{Fe,X1:Va} + 2({}^{1}L_{Fe,X1:Va}) + 3({}^{2}L_{Fe,X1:Va})) + ({}^{0}L_{Fe,X2:Va} + \\ 2({}^{1}L_{Fe,X2:Va}) + 3({}^{2}L_{Fe,X2:Va})) - ({}^{0}L_{X1,X2:Va}) - (L_{Fe,X1,X2:Va})\ \}/RT\end{aligned} \tag{S13}$$

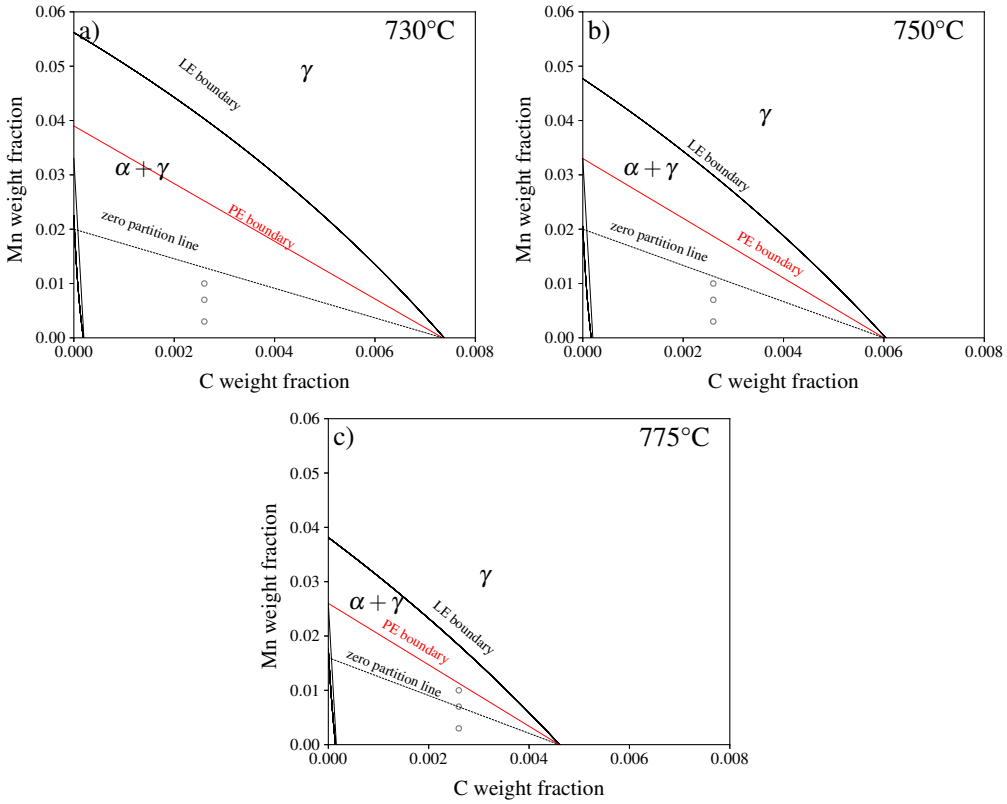

Figure S2: Isothermal sections of the Fe-C-Mn at a) 730°C, b) 750°C and c) 775°C showing the different possible growth modes (LEP-LENP and PE) for the studied compositions (grey circles).

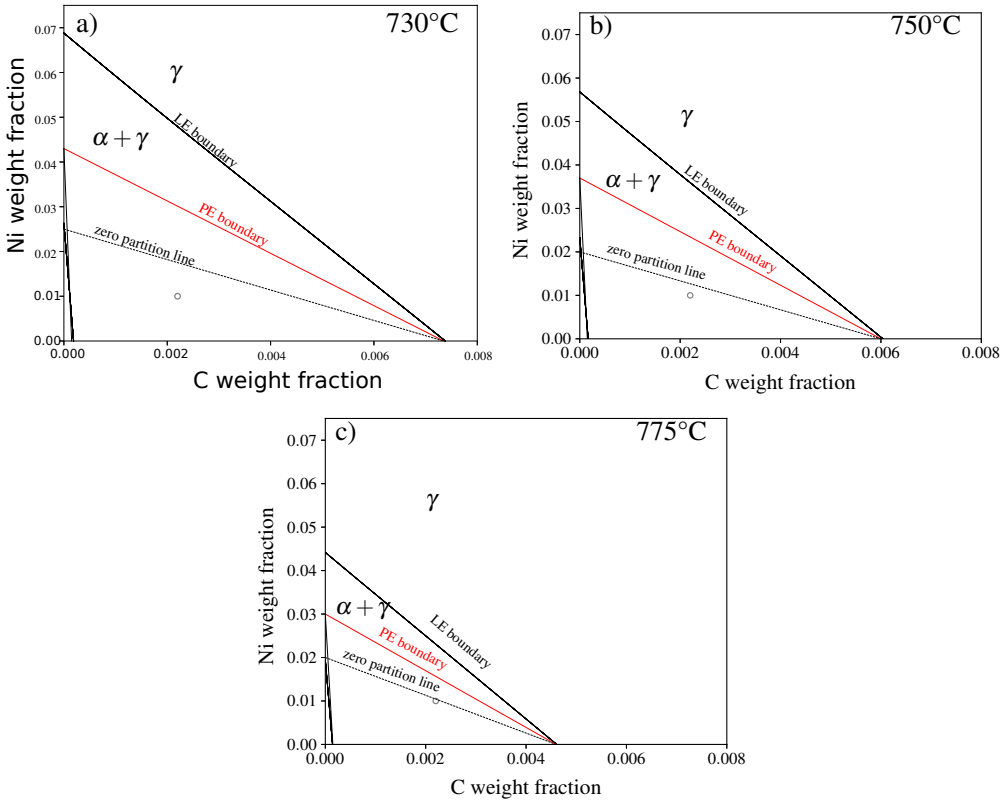

Figure S3: Isothermal sections of the Fe-C-Ni at a) 730°C, b) 750°C and c) 775°C showing the different possible growth modes (LEP-LENP and PE) for the studied compositions (grey circles).

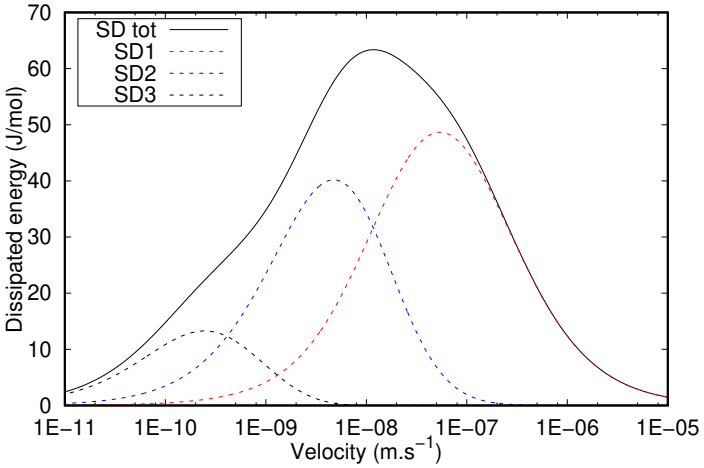

Figure S4: The dissipated free energy due to Ni diffusion across the interface as function of the interface velocity for the Fe-0.22C-1Ni at 730°C.

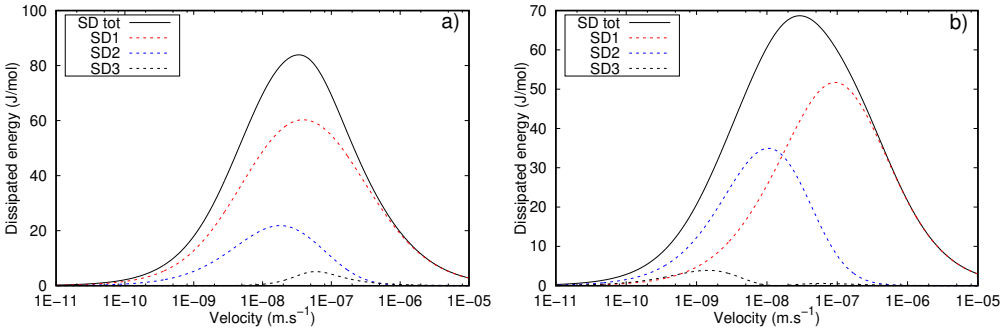

Figure S5: Dissipated free energy due element X (a. Mo and b. Cr) diffusion across the interface as function of the interface velocity for Fe-0.26C-0.2Mo at 730°C and Fe-0.26C-1Cr at 750°C, respectively.

Table S1: All the parameters used in the solute drag modeling for different Fe-C-X systems at different tables. TCFE9 and MOB2 databases of ThermoCalc and DICTRA were used to calculate the different thermodynamic properties in austenite and ferrite such as chemical potentials and diffusion coefficients.

T(°C)	Fe-C-X	${}^0L_{Fe,X:Va}$ $(kJ.mol^{-1})$	E_b $(kJ.mol^{-1})$	${}^0L_{Fe:C,Va}$ $(kJ.mol^{-1})$	$L_{Fe,X:C,Va}$ $(kJ.mol^{-1})$	ϵ_{XC}	D_{int} $(m^2.s^{-1})$
730	0.3Mn	-1.4	+1.5	50	-12.7	-5.0	5.17E-18
750	0.3Mn	-1.6	+1.5	50	-13.1	-4.9	1.03E-17
775	0.3M	-1.9	+1.5	50	-13.5	-4.7	2.36E-17
730	0.7Mn	-1.5	+1.5	50	-12.8	-5.0	5.34E-18
750	0.7Mn	-1.7	+1.5	50	-13.2	-4.9	1.06E-17
775	0.7Mn	-2.0	+1.5	50	-13.6	-4.7	2.47E-17
730	1Mn	-1.7	+1.5	50	-13.1	-5.0	5.46E-18
750	1Mn	-1.8	+1.5	50	-13.3	-4.9	1.08E-17
775	1Mn	-2.1	+1.5	50	-13.7	-4.7	2.45E-17
730	1Ni	-11.7	-6.5	50	-18.2	4.73	1.13E-18
750	1Ni	-11.8	-6.5	50	-18.4	4.66	2.38E-18
775	1Ni	-11.9	-6.5	50	-18.5	4.58	5.79E-18
730	0.2Mo	-7.2	-15	50	-33.1	-12.5	9.6E-18
750	0.2Mo	-7.5	-15	50	-33.1	-12.2	1.82E-17
775	0.2Mo	-7.9	-15	50	-33.1	-11.9	3.94E-17
750	1Cr	+5.1	+1.5	50	-13.2	-11.6	4.29E-18
775	1Cr	+4.9	-1.5	50	13.3	-11.3	1.09E-17

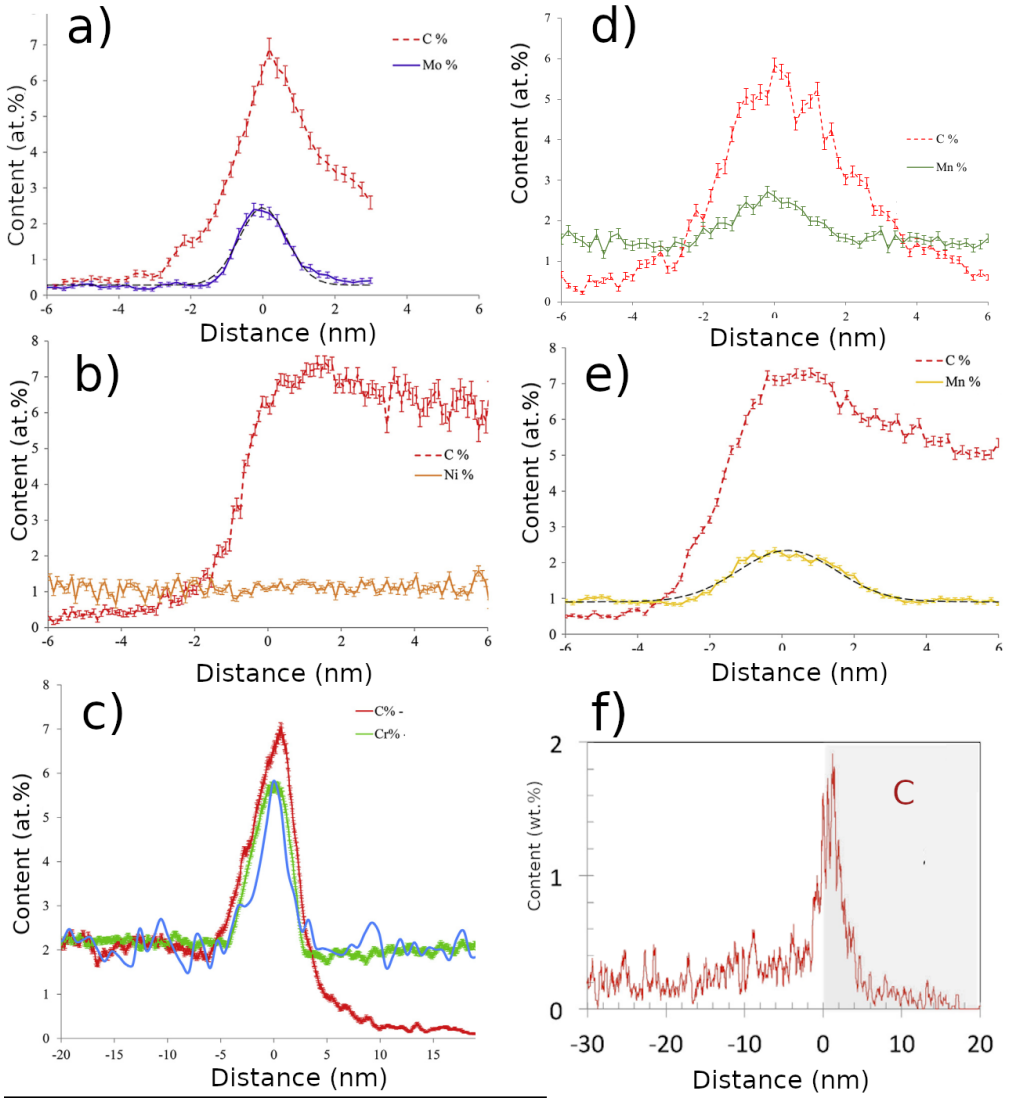

Figure S6: Different APT measurements showing carbon and X element distribution across a ferrite marteniste interface in different Fe-C-X systems, a) Fe-C-Mo [43], b) Fe-C-Ni[43], c) Fe-C-Cr [43] and d-f) Fe-C-Mn [43, 25].

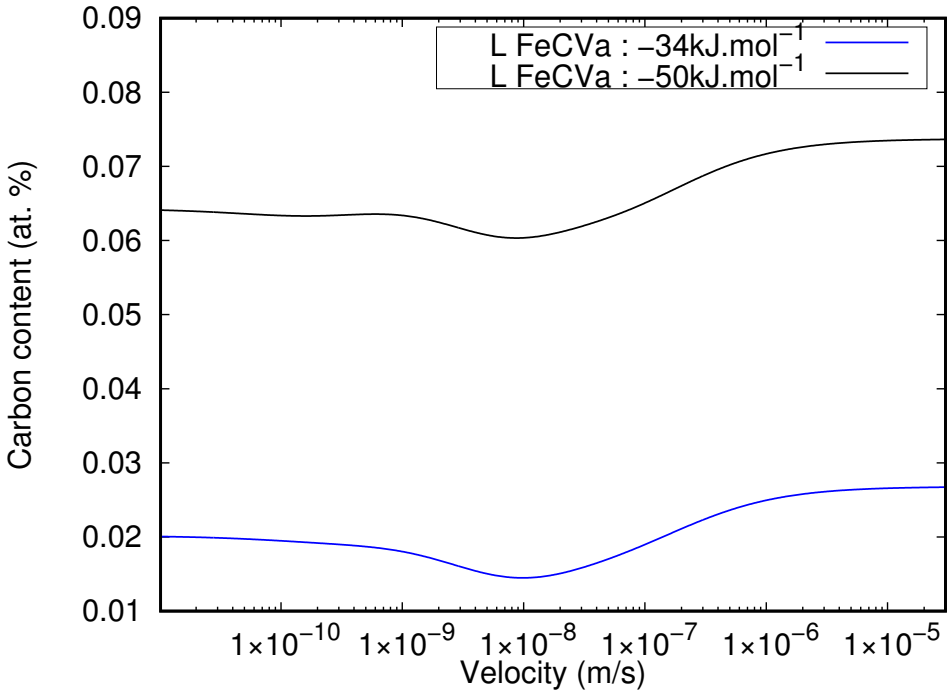

Figure S7: Carbon content evolution at the inteface as a function of interface velocity, calculated using the solute drag model for two different L(Fe:C,Va) parameters.